MIRL REPORT NO. 76

# A STUDY OF FACTORS SUSPECTED OF INFLUENCING THE SETTLING VELOCITY OF FINE GOLD PARTICLES

Daniel E. Walsh
Dr. P.D. Rao

Mineral Industry Research Laboratory
University of Alaska Fairbanks
Fairbanks, Alaska 99775-1180

*Library of Congress Cataloging in Publication Data*

Library of Congress Catalog Card Number 88-060573
ISBN 0-911043-05-5

January, 1988

Published by

Mineral Industry Research Laboratory
210 O'Neill Research Laboratory
University of Alaska Fairbanks
Fairbanks, Alaska 99775-1180

# ABSTRACT

In this study, the authors used a radiotracer detection system coupled to a frequency counter and the radioisotope, $^{198}Au$, to investigate the effect of several variables on the terminal settling velocity of gold particles. The settling velocities of 35 manufactured gold particles (97 mg to 0.03 μg) were determined in order to produce working gold settling velocity vs. size-shape graphs for practical engineering application.

Additionally, eight gold spheres were progressively flattened through 3 stages. At each flatness stage their settling velocity was determined. This highlighted the effect on settling velocity of decreasing shape factor for particles of constant mass (97 mg to 0.6 μg). The settling velocities of natural gold particles were also determined and compared to those of the corresponding manufactured particles.

Finally, a generalized randomized block design was generated to explore the effects of three variables on the settling velocity of gold grains. The design was to be blocked according to gold size- shape combinations. The three variables (factors) studied were water temperature, clay concentration in the fluid, and the clay mineralogy of the suspended clays. This design was analyzed using a fixed effects analysis of variance model. The analyses show that all three factors had a significant ($p < 0.001$) influence on the settling velocity of gold particles. The data suggest that the clay mineralogy (viscosifying properties) of suspensions is perhaps the most influential parameter with respect to settling velocity determination.

## ACKNOWLEDGEMENTS

The Mineral Industry Research Laboratory of the University of Alaska, Fairbanks and the authors wish to acknowledge the United States Bureau of Mines funding of this project (Research Grant No. 1154102). In addition, they also thank the following persons for their advice and/or contributions to the study.

John Bradbury, Glassblower, Institute of Marine Science, University of Alaska, Fairbanks.

Jim Carni, Research Reactor Facility, University of Missouri, Columbia.

Dan Holleman, Radiobiologist, Institute of Arctic Biology, University of Alaska, Fairbanks

Dave Maneval, Professor of Mineral Preparation Engineering, USBM Project Coordinator, School of Mineral Engineering, University of Alaska, Fairbanks.

Ed McLaughlin, Mechanical Technician, School of Mineral Engineering, University of Alaska, Fairbanks.

William P. Miller, Assistant Director Nuclear Reactor, University of Washington, Seattle.

Gil Mimken, Electronics Support Engineer, Institute of Marine Science, University of Alaska, Fairbanks.

Carl Overpeck, Graduate Student, Environmental Quality Engineering Department, University of Alaska, Fairbanks.

Steve Teller, Graduate Student, Geology Department, University of Alaska, Fairbanks.

Dana Thomas, Professor of Mathematical Statistics, University of Alaska, Fairbanks.

Staff, Electronics Shop, Geophysical Institute, University of Alaska, Fairbanks.

Staff, Mineral Industry Research Laboratory, University of Alaska, Fairbanks.

# TABLE OF CONTENTS

# LIST OF FIGURES

## LIST OF FIGURES (Continued)



## LIST OF TABLES

## DEFINITION OF SYMBOLS

| Symbol | Units | Definition |
|---|---|---|
| a,A | mm, μm | Major axis length of particle |
| b,B | mm, μm | Intermediate axis length of particle |
| c,C | mm, μm | Minor axis length of particle |
| $C_D$ | — | Drag coefficient |
| $C_s$ | mg/liter | Suspended solids concentration |
| $C_w$ | — | Percent by weight solids concentration |
| CSF | — | Corey's Shape Factor |
| d | mm, μm | Spherical particle diameter |
| $d_c$ | mm, μm | Diameter of a circle equal in area to the largest projected area of a particle |
| $D_c$ | mm, μm | Diameter of the smallest circle which encloses the largest projected area of a particle |
| $d_n$ | mm, μm | Nominal diameter. The diameter of a sphere which has a volume equal to that of the particle |
| D | cm, mm | Inside diameter of a pipe, tube, etc. |
| (dv/dy) | $sec^{-1}$ | Shear rate |
| F | lb/100 $ft^2$ | Fann shear stress |
| g | $cm/sec^2$ | Acceleration of gravity |
| h | cm, mm | Height above a referenced datum |
| Δh | cm, mm | Fall distance |
| K | — | Heywood's volume constant |
| $K_f$ | — | Coefficient of flattening defined by Saks |

# DEFINITION OF SYMBOLS

| Symbol | Units | Definition |
|---|---|---|
| $n$ | — | Number of observations |
| $Q$ | $cm^3/sec$ | Volume flow rate |
| $R$ | rpm | Fann shear rate |
| $Re$ | — | Reynolds number |
| $t$ | sec | Time interval |
| $t(\alpha/2(x),\nu)$ | — | Student's t score at level of significance ($\alpha/2(x)$) and $\nu$ degrees of freedom |
| $V_t$ | cm/sec | Terminal settling velocity |
| $V_Q$ | cm/sec | Flow velocity |
| $x$ | — | Variable coefficients |
| $\alpha$ | — | Statistical level of significance |
| $\gamma_m$ | — | Specific gravity of a suspension |
| $\gamma_s$ | — | Specific gravity of a solid |
| $\mu$ | centipoise $(gm/cm \cdot s)x10^{-2}$ | Dynamic viscosity |
| $\mu_a$ | centipoise | Apparent dynamic viscosity at shear rate, dv/dy |
| $\nu$ | — | Statistical degrees of freedom |
| $\pi$ | — | Pi |
| $\rho_f$ | $gram/cm^3$ | Density of liquid |
| $\rho_m$ | $gram/cm^3$ | Density of suspension |
| $\rho_s$ | $gram/cm^3$ | Density of solid |
| $\tau$ | $dynes/cm^2$ | Shear stress |

# INTRODUCTION

Recent years have seen the development of controversy between the Alaskan placer mining industry and state and federal environmental regulatory agencies. The major issue has been the quality and impact of the discharge of mine effluent waters used for processing the placer ores. Regulatory agencies have suggested that the most practical way for miners to comply with the current effluent standards is for mines to modify their recovery systems to employ high recycle of their process water and perhaps even to adopt zero discharge operations. Miners contend that the high recycle of plant waters is accompanied by the build up of suspended solids in the fluid and that this increase of suspended solids lowers gold recovery by conventional sluice box recovery systems.

Evidence given at EPA hearings suggests that the use of recycled placer plant water may lower gold recovery by as much as 30%. However, a recent study performed for Alaska's Department of Environmental Conservation failed to show a significant effect on gold recovery by water containing a large amount of suspended solids[1]. This study looked at the recovery of 30 x 70 mesh gold using a small test sluice (6 inches wide x 8 feet long) and water containing as high as 200,000 mg/liter suspended solids. Nevertheless, the placer mining industry maintains that gold recovery is lowered with recycled water and contends that the DEC study failed to show this due to the size and shape of the gold used and because of the limited size of the sluice box and the small quantity of material processed per test. Miners cite the effects of the increase of fluid viscosity, fluid specific gravity, and possible clay-gold surface phenomena on the settling velocity of fine gold as reasons for poorer gold recovery where recycled plant water is used.

These arguments by both miners and regulators indicated the need for a detailed scientific study of the influence of suspended solids on the settling velocity of fine gold. The recent development by the Mineral Industry Research Laboratory (MIRL) of the University of Alaska, Fairbanks, of a gold detection system employing the gold radioisotope $Au^{198}$, improved the feasibility of such a study[2]. Previous gold settling velocity work has been done[3,4,7,8] as has work with the settling velocity of other minerals[5,6,7,11,12]. All of these studies, however, relied on theoretical settling velocity calculations or used optical measurement methods which restricted them to fairly coarse particle sizes (≥ 2mg gold) and to clear water conditions. The present study removed both of these restrictions due to the radiotracer technique employed.

In addition to extending the scope of previous settling velocity work and confirming its accuracy, MIRL desired to provide, from direct measurement, gold settling velocity data which could be used for recovery plant design. Such data should be of considerable use to the mineral processing industry due to the range of particle sizes and shapes studied, and because much of data was obtained for particles which settled at velocities placing them in the transitional settling velocity range; that range which lies between the Stokes and Newtonian settling regimes. Additionally, that portion of this study which focused on the effects of clay mineralogy and clay concentration on the settling velocity of gold particles has provided useful results and pointed to the need for additional work in this area.

# BACKGROUND INFORMATION REVIEW

### Settling Velocity Theory

A useful concept in understanding the characteristics of gold particles and of associated minerals found in the various alluvial placer deposits throughout the world is that of hydraulic equivalence. According to Tourtelot[7], hydraulic equivalence is the concept that describes the relationship between different mineral grains of varying size and specific gravity which are deposited in the same hydrodynamic environment. Mineral grains are said to be hydraulically equivalent if they have the same settling velocity under the same conditions. In some Soviet literature the term "hydraulic size" is used as a synonym for settling velocity.

Sedimentation theory, and hence the concept of hydraulic equivalence, are based on the laws of fluid mechanics. These laws are derived for spherical particles and consider a balance of buoyant, gravitational, and viscous drag forces acting upon particles.

Stokes' Law states that settling velocity increases as the square of the diameter of the particle. With decreasing particle size the settling velocity drops off very rapidly. Settling velocity also varies with density. This law is applicable for particles with Reynolds numbers (Re) less than one; for particles so small that the liquid flows around them in a laminar fashion:

$$Re = \frac{V_t d \rho_l}{\mu} \qquad \text{Eq. 1}$$

Stokes' Law is then stated as:

$$V_t = \frac{g(\rho_s - \rho_l)d^2}{18\mu} \qquad \text{Eq. 2}$$

Newton's Law applies to coarser spherical particles that settle in the turbulent flow regime. Newton's Law states that terminal velocity varies as the square root of the diameter

of a particle. Consequently increase in settling velocity is not as rapid with size as it is with Stokes' Law. This law applies to particles with Reynolds numbers greater than 1,000. For Newton's Law:

$$V_t = \left[ \frac{3.33\, g\, (\rho_s - \rho_l) d}{\rho_l} \right]^{1/2} \qquad \text{Eq. 3}$$

Between the ranges of Stoke's Law and Newton's Law, there is no single equation that can be applied to calculate settling velocity. Such settling velocities can be determined indirectly, by iteration, using the equation:

$$V_t = \left[ \frac{4g\, (\rho_s - \rho_l) d}{3\, C_D \rho_l} \right]^{1/2} \qquad \text{Eq. 4}$$

The drag coefficient, $C_D$, is a function of particle shape and the flow characteristics about the particle. Values of $C_D$ are generally available in graphical form as plots of $C_D$ vs. the Reynolds number for given shapes. Such a graph is shown in Figure 1.

An alternative approach to the iterative method of solving for transitional settling velocities of spheres is provided by Wasp [9]. Equations 5, 6, and 7 provide the basis for his approach:

$$C_D = \frac{4g\, (\rho_s - \rho_l) d}{3\, \rho_l V_t^2} \qquad \text{Eq. 5}$$

$$\frac{C_D}{Re} = \frac{4g\, (\rho_s - \rho_l) \mu}{3\, \rho_l^2 V_t^3} \qquad \text{Eq. 6}$$

$$C_D Re^2 = \frac{4g\, (\rho_s - \rho_l) \rho_l d^3}{3\, \mu^2} \qquad \text{Eq. 7}$$

Wasp notes that Eq. 6 is independent of particle diameter while Eq. 7 is independent of a particle's terminal settling velocity and states that the equations are general and apply over the whole range of Reynolds numbers.

With the aid of graphs of $C_D/Re$ and $C_D Re^2$ as functions of Re for spherical particles (Figure 2) and Eq. 6 and Eq. 7, transitional settling velocities and/or drag coefficients may be determined. For example, if one desires a particle's terminal setting velocity, given only a spherical particle diameter, $C_D Re^2$ may be calculated using Eq. 7. This calculated value may then be used with Figure 2 to find Re. The final step requires rearrangement of Eq. 1 to solve for the terminal settling velocity, $V_t$.

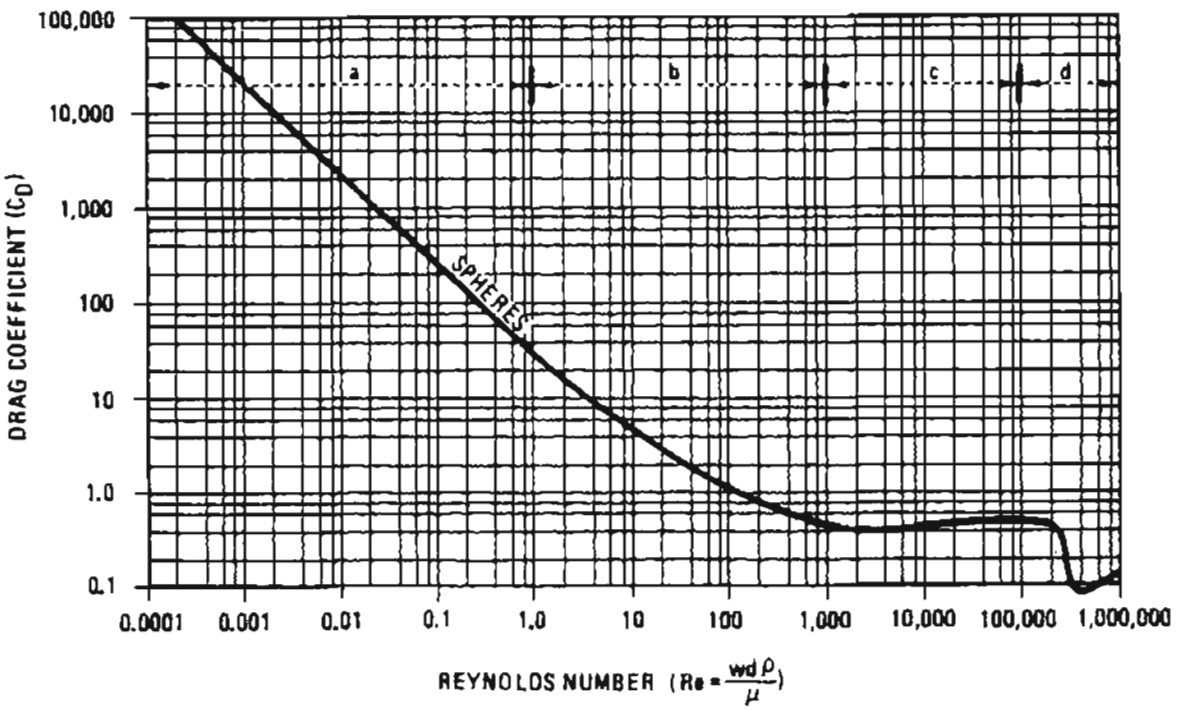


**Figure 1. Drag coefficient ($C_D$) for spheres as a function of the Reynolds Number[9].**

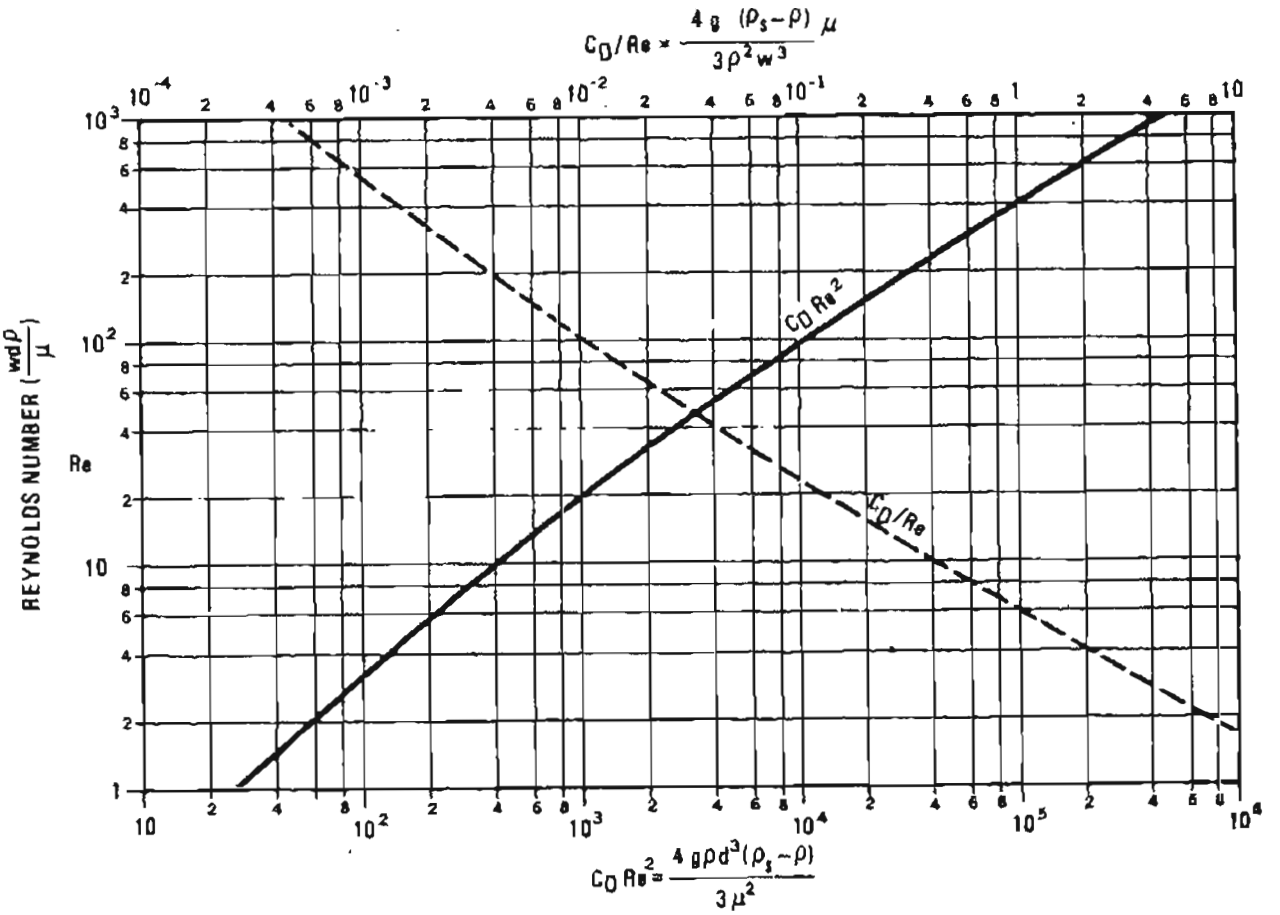


**Figure 2. $C_D/Re$ and $C_D Re^2$ versus Re for spheres[9].**

**Measures of Particle Shape**

Not only does the size and specific gravity of a mineral grain affect its settling velocity, but shape too has a pronounced influence. For particles which obey Stokes' Law, the effect of particle shape is proportional to the degree that the grain shape departs from that of a sphere (Tourtelot[7]). Several ways exist of describing the non-sphericity of particles and the more common ones are listed below. In describing these, the following convention of particle dimensions is adopted: A≥ B≥ C, so that for nonequidimensional grains, C corresponds to the grain thickness and A and B dimension of the grain's surface of largest projected area.

(1) The Flatness Factor[4] is defined as: FF = (A+B)/2C and can be thought of as the arithmetic average of the two largest dimensions divided by the particle thickness. The flatness factor equals 1 for a sphere or cube and gets progressively larger as particles become flattened.

(2) Heywood's shape constant[10], K:

$$K = \frac{\text{Particle Volume}}{(\text{projected diameter})^3}$$

where the projected diameter is defined as $(4(AB)/\pi)^{0.5}$. K equals 0.524 for a sphere and becomes smaller as the flatness of the particle increases.

(3) Coefficient of flattening, $K_f$, is defined by Saks[6] as: $K_f = \sqrt{AB}/C$.

(4) Corey's Shape Factor[11] is defined as: C.S.F. = $C/\sqrt{AB}$ and can be thought of as the particle thickness divided by the geometric average of the particle's other two dimensions. Corey's shape factor equals 1 for a cube or sphere and decreases as the flatness of a grain increases.

Corey discusses the measure of shape which bears his name as follows:

"The shape factor $c/\sqrt{ab}$ is probably not as complete from the theoretical standpoint as the volume constant of Heywood because it does not take roundness into account. Furthermore, the value for both spheres and cubes is 1.0, therefore this shape factor

cannot accurately be called a sphericity. However, it has a decided advantage in that it does not involve the tedious and time consuming process of measuring surface or sectional areas of irregular particles and yet it does describe the flatness. For this reason the ratio $c/\sqrt{ab}$ was used to express shape in this study.

Other ratios were considered for use in this investigation but were eliminated because of theoretical and practical considerations. One of these is the ratio $\{(b/a + c/a + c/b)/3\}$ which seemed to have no advantage over the ratio $c/\sqrt{ab}$ and is less convenient. Another was the ratio $d_n/\sqrt{ab}$ which was eliminated because it gives a value for spheres less than the value for cubes. The ratio $c/d_n$ was not used because an angular particle can give a high value to a non-spherical particle.

A shape factor analogous to the volume constant of Heywood (1:27) was considered. Heywood's volume constant is expressed by the ratio:

$$k = \text{volume}/d^3$$

where d is the diameter of a circle having an area equal to the largest projected area of the particle. The possibility of replacing $d^3$ with $(ab)^{3/2}$ was studied since $(ab)^{1/2}$ is roughly related to d. However, $(ab)^{1/2}$ is normally somewhat greater than d and the discrepancy is considerable in the case of round particles which should have higher values of the ratio if it is to correlate with fall velocity.

It is not probable that a simple ratio can be found that adequately expresses shape from the theoretical point of view. However, it is believed that the shape factor used in this study is superior to the simplified ratio suggested by Wadell (9:264):

$$d_c/D_c$$

where $d_c$ is the diameter of a circle equal in area to the largest projected area and $D_c$ is the diameter of the smallest circle circumscribing this area. this ratio not only gives values of shape for disks and spheres that are identical, but it also is difficult to measure."

Albertson[12] concluded that while it was unlikely that particle shape could ever be fully described by a single parameter, Corey's shape factor adequately described particle shape to the degree of refinement required to discuss a particle's shape influence on settling velocity. The authors of the present study chose to use Corey's shape factor for the above quoted reasons and because Corey's shape factor has consistently been used in previous MIRL studies involving gold shape since 1973.

**Effects of Shape on Settling Velocity**

The effect of particle shape on the settling velocity of constant mass particles can be seen by examining Figure 3. This data, compiled by Corey, shows that particles with a shape factor of 0.85 have an average terminal settling velocity of nearly twice that seen for particles of shape factor 0.35. Spherical particles settled at velocities three times those observed for particles of 0.35 shape factor. The size range of particles studied by Corey was 4 mesh to 14 mesh (4.8mm to 1.4mm).

In summarizing Corey's work as well as that of other researchers, Albertson developed the graph of $C_D$ vs Re for different shape factors shown in Figure 4. Both $C_D$ and Re have been defined by Albertson as:

$$C_D = \frac{4g(\rho_s - \rho_l)d_n}{3\ \rho_l V_t^2} \qquad \text{Eq. 8}$$

$$Re = \frac{V_t d_n \rho_l}{\mu} \qquad \text{Eq. 9}$$

These definitions are identical to Equations 5 and 1 respectively in all respects except that $d_n$, nominal diameter, is used in place of d, spherical diameter. Nominal diameter is defined as the diameter of a sphere having the same volume as the particle itself.

Using Figure 4 and equations 2, 3, and 4 one can calculate settling velocities for particles of different shape factors. The option exists to use the values of Figure 4 and the approach of Wasp to construct $C_D/Re$ and $C_D Re^2$ vs Re plots for each shape factor. This would allow more rapid evaluation of settling velocities for particles settling in the transitional range.

With respect to the effect of shape on the settling velocity of gold particles, Shilo and Shumilov[4] have presented the data shown in Table 1 and Figure 5. These Soviet scientists measured the settling velocity of gold spheres of mass ranging from 600 mg to 2 mg. They then progressively flattened these spheres to obtain particles with lower Corey shape factors and larger sieve sizes, measuring the settling velocity at each stage of flatness. It is quite clear that although each particle remained constant in mass, their settling velocity was significantly decreased by even a slight

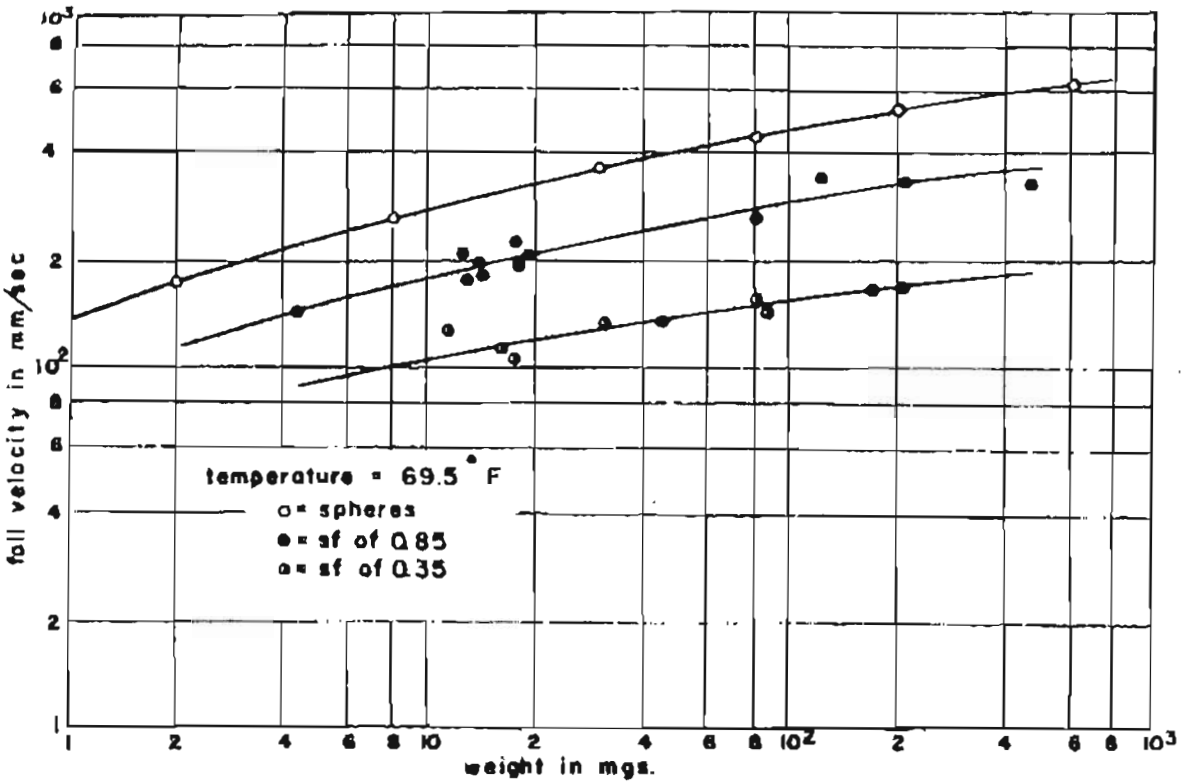


Figure 3. Fall velocity as a function of particle shape and mass[11].

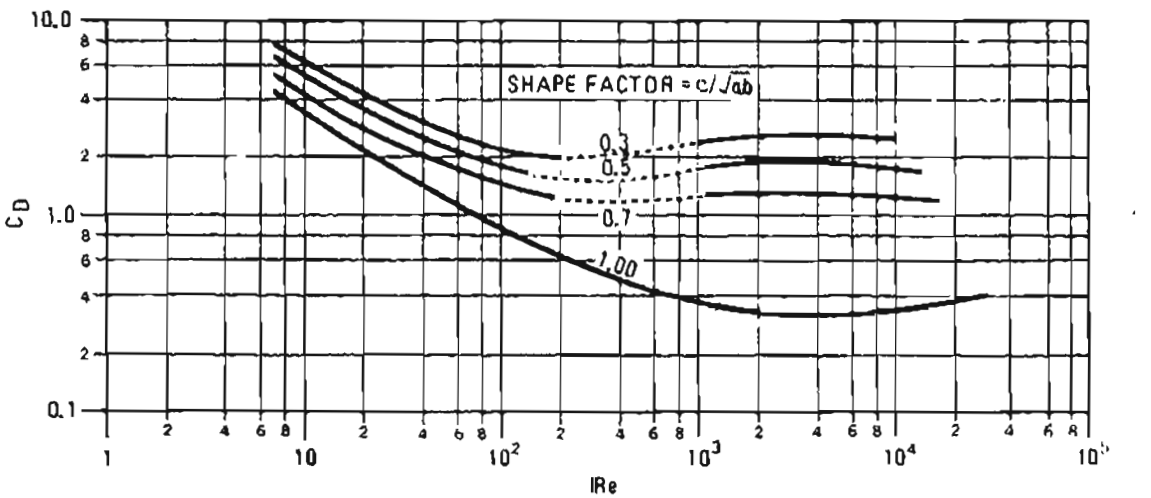


Figure 4. Drag coefficient versus Reynolds Number for different Corey's Shape Factors[9].

Table 1
Main characteristics of gold particles used in Soviet laboratory settling velocity experiments[4].

| Particle No. | Particle Wt. (mg) | Particle Flatness Factor (FF) Beginning of Test | End of Test |
|---|---|---|---|
| 1 | 586 | 1 | 47.5 |
| 2 | 316 | 1 | 42.6 |
| 3 | 122 | 1 | 38.3 |
| 4 | 79 | 1 | 47.9 |
| 5 | 57 | 1 | 47.9 |
| 6 | 28 | 1 | 59.0 |
| 7 | 20 | 1 | 54.7 |
| 8 | 9 | 1 | 51.4 |
| 9 | 5 | 1 | 48.6 |
| 10 | 2 | 1 | 35.3 |

FF = (A+B)/2C A,B, and C are length, width, and thickness respectively

increase in their flatness. Shilo and Shumilov note that the settling velocity of large flat particles may be the same as that of small, but more spherical ones. They continued their work by looking at the gold from 12 placer deposits in the northeastern part of the Kolyma region and found that native placer gold particles of various sizes and shapes followed the same pattern as shown for their laboratory results (Figure 6).

**Densities and Viscosities of Clay Water Suspensions**

A review of the basic settling velocity equations presented in an earlier section shows that for solid particles the primary parameters affecting settling velocity, other than the particle's density, shape and nominal diameter, are the density and viscosity of the liquid or suspension. These two physical properties of suspensions are discussed in this section.

According to Wasp[9], there are three density terms involved in the specification of any suspension; namely, the density of the particles, the density of the suspending medium, and the density of the suspension itself. Suspension densities may be measured directly using hydrometers, specific gravity bottles, pulp density scales, and other conventional techniques. Alternatively, the density of a suspension of a given concentration may be calculated if the densities of the fluid and the suspended solids are known. The density of a suspension in terms of its component densities is given by equation 10.

$$\rho_m = \frac{100}{\frac{C_w}{\rho_s} + \frac{100-C_w}{\rho_l}} \qquad \text{Eq. 10}$$

$C_w$ is the concentration of solids in percent by weight. When dealing with water-clay suspensions, it is often more convenient to define solids concentrations in terms of the suspended solids units, mg/liter. Equation 10 may be rewritten as:

$$\frac{\rho_m}{\rho_l} = \left[ \frac{\frac{C_s \rho_l}{\rho_s} - C_s}{10^6} + 1 \right]^{-1} \qquad \text{Eq. 11}$$

where $C_s$ is suspended solids concentrations in mg/liter. Equation 11 may be further reduced if terms of specific gravity are substituted for the density terms:

$$\gamma_m = \left[ \frac{\frac{C_s}{\gamma_s} - C_s}{10^6} + 1 \right]^{-1} \qquad \text{Eq. 12}$$

Figure 7 shows plots of Equation 12 for various specific gravity solids.

From a theoretical point of view, the effect of increasing suspension density on the terminal settling velocity of a gold particle can be seen by rearranging Eq. 8 to yield:

$$V_t = \left[ \frac{4g(\rho_s - \rho_m) d_n}{3 C_D \rho_m} \right]^{1/2} \qquad \text{Eq. 13}$$

An increase in $\rho_m$ decreases the numerator and increases the denominator. $C_D$ will undoubtably be altered given a change in suspension density. In the case of Stokes' settling the ratio of settling velocities of a particle in a suspension of $\rho_m^o$ compared to that of $\rho_m'$, given , $\rho_m' > \rho_m^o$ is described by:

$$\frac{V_t^o}{V_t'} = \frac{(\rho_s - \rho_m^o)}{(\rho_s - \rho_m')} = \frac{(\gamma_s - \gamma_m^o)}{(\gamma_s - \gamma_m')} \qquad \text{Eq. 14}$$

For the Newtonian settling regime, this same ratio of settling velocities is given by:

$$\frac{V_t^o}{V_t'} = \left[ \frac{(\rho_s - \rho_m^o)\rho_m'}{(\rho_s - \rho_m')\rho_m^o} \right]^{1/2} = \left[ \frac{(\gamma_s - \gamma_m^o)\gamma_m'}{(\gamma_s - \gamma_m')\gamma_m^o} \right]^{-1/2} \qquad \text{Eq. 15}$$

How would a change in suspension density affect a gold sphere's ($\gamma_s$ = 18.0) settling velocity? As an example, consider a change in fluid density from that of water at standard condition ($\gamma_m^o$ = 1.00) to that of water at standard conditions with a suspended solids ($\gamma_s$ = 2.65) concentration of 50,000 mg/l. Equation 12 yields $\gamma_m'$ equal to 1.032. Using these values of $\gamma_m^o$ and $\gamma_m'$ in Equations 14 and 15 gives:

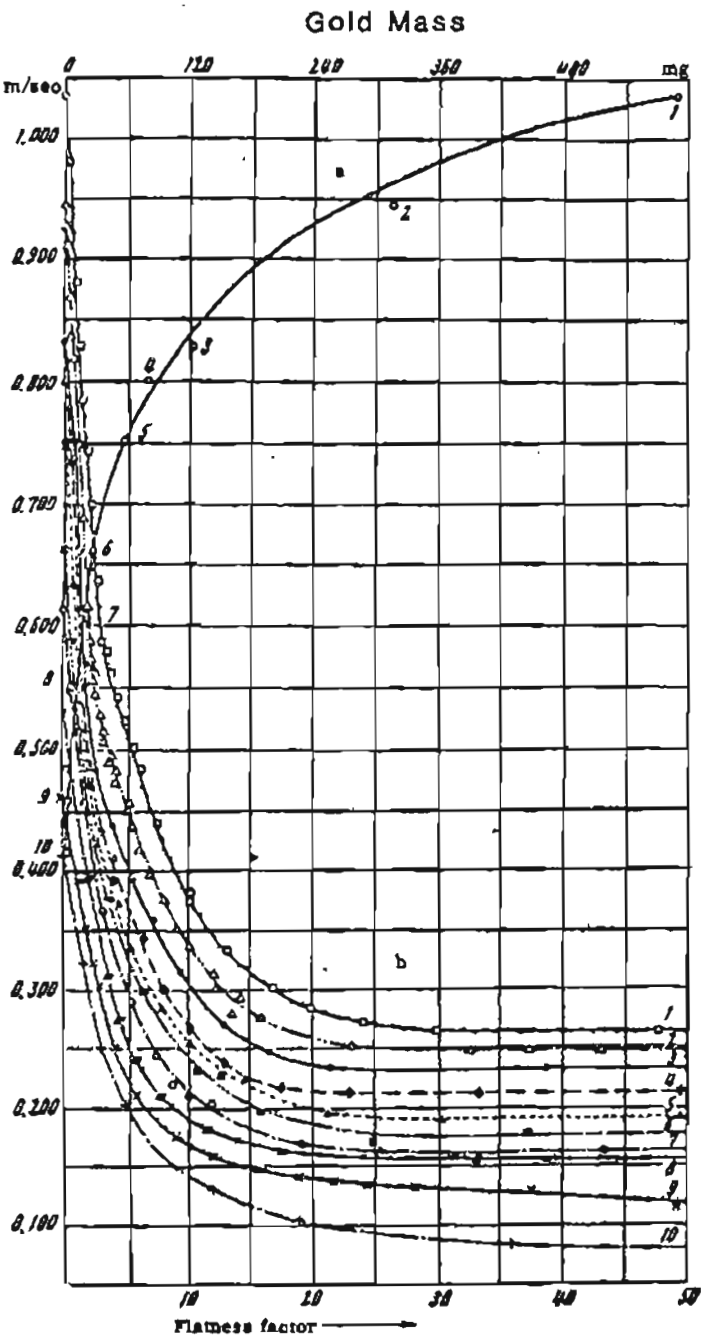


Figure 5. Mass of gold particles (a) and their settling velocity (b) versus their flatness factor[4].

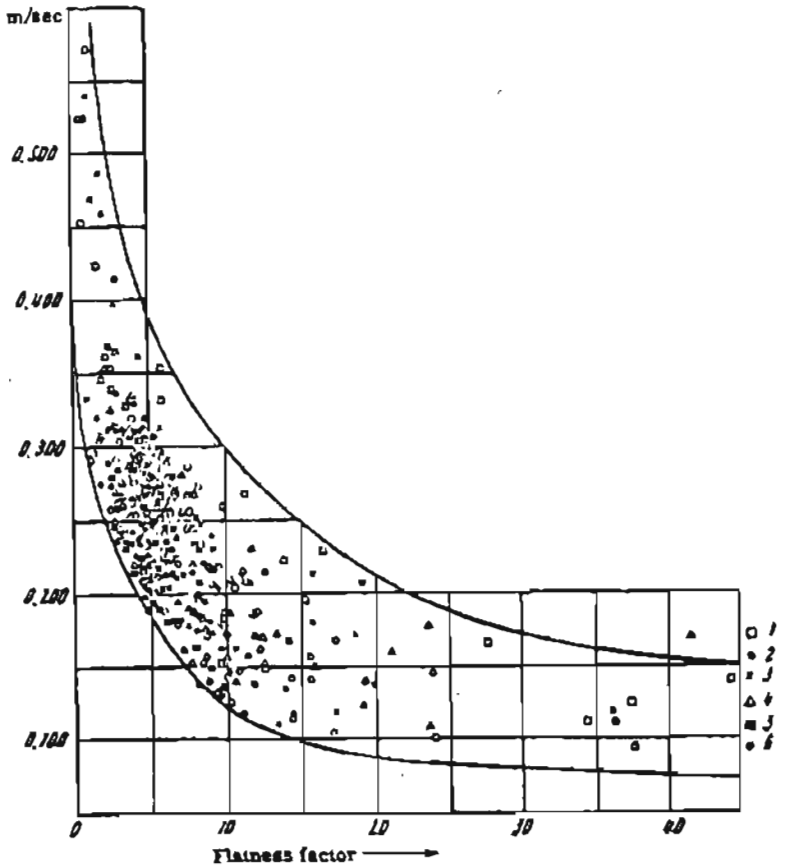


**Figure 6. Settling velocity of natural gold particles versus their flatness factor. Gold from six placers in the northeastern Kolyma region[4].**

$V_t^o / V_t' = 1.002$ for Stokean Settling

$V_t^o / V_t' = 1.017$ for Newtonian Settling

Thus a gold particle's settling velocity is reduced as the suspension density is increased. With the assumed density changes in the above example, this decrease ranges from 0.2% for Stokes' settling to 1.7% for Newtonian settling. The percent decrease in settling velocity for particles settling in the transitional regime should fall between these values, i.e. 0.2% ≤ transitional regime % decrease ≤ 1.7%. Non-spherical particles should be similarly affected by changes in suspension density.

Unlike suspension density, the viscosity of a suspension is not related only to the suspended solids concentration. It is a function of the suspended particles' size, shape, and mineralogy, and the suspension temperature as well. Viscosity of a fluid is a measure of its internal resistance to movement. Molasses, for instance, is more viscous than water. Viscosity is defined in terms of the shear stress-shear rate relationship for the fluid. Shear stress and shear rate are physical concepts that pertain to the deformation of matter.

For some fluids shear stress ($\tau$) is directly proportional to shear rate ($dv/dy$). A fluid of this type is called Newtonian. Water is a Newtonian fluid. Newtonian fluids satisfy the differential equation:

$$\tau = \mu \, (dv/dy) \qquad \text{Eq. 16}$$

where $\mu$ is some constant. The graph of this equation is a straight line through the origin (Figure 8a).

The viscosity of a fluid is defined to be shear stress divided by shear rate. Thus, the viscosity of the fluid described by the preceding equation is $\mu$. The viscosity of a Newtonian fluid is constant. If we plot it as a function of shear rate, we get a horizontal line (Figure 8b).

There is an important group of fluids whose shear diagrams or rheograms, as the shear stress-shear rate curves are called, do not conform to Equation 16. These fluids, for which the rheogram is not linear through the origin, are known as non-Newtonian fluids. Typical of this group are a great many suspensions of solids in water.

Figure 8c is a rheogram for a typical clay-water suspen-

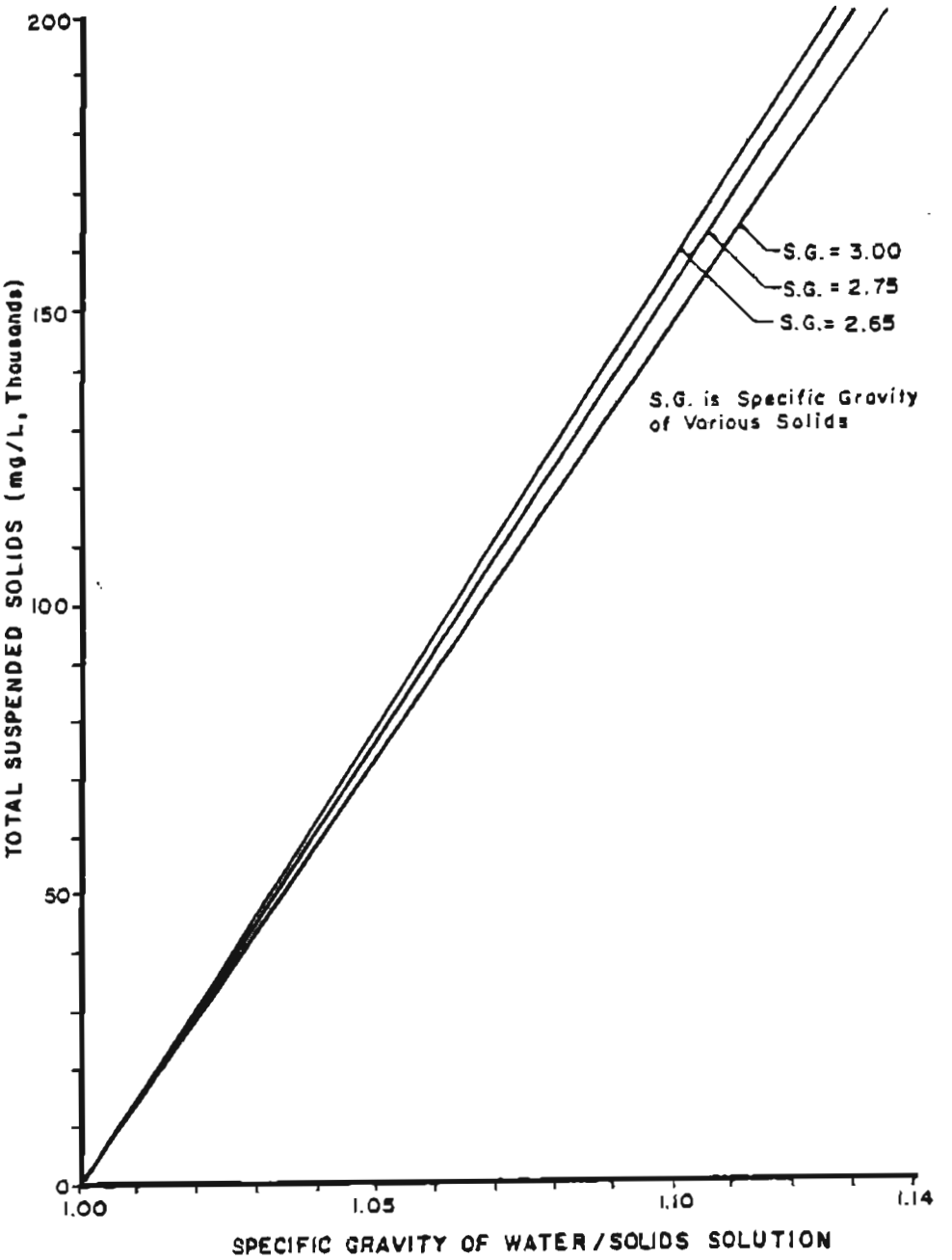


Figure 7. Theoretical relationship between suspended solids concentration and suspension specific gravity[1].

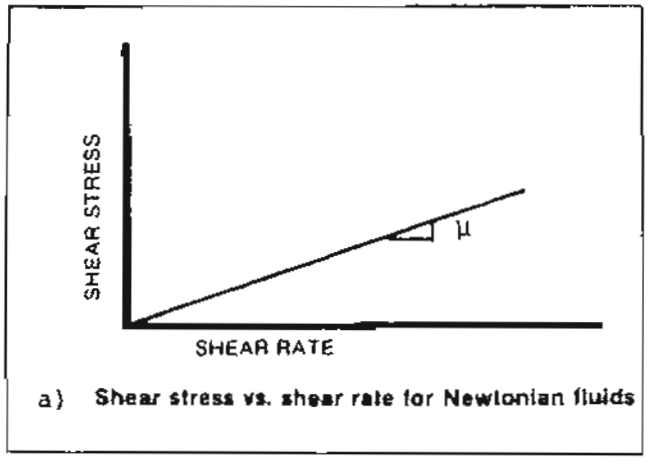


a) Shear stress vs. shear rate for Newtonian fluids

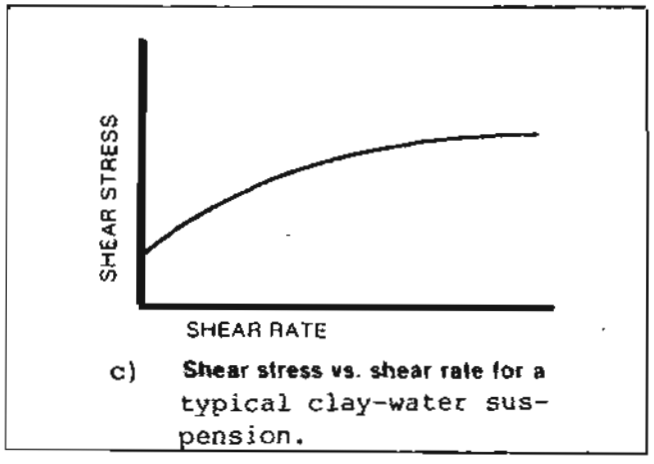


c) Shear stress vs. shear rate for a typical clay-water suspension.

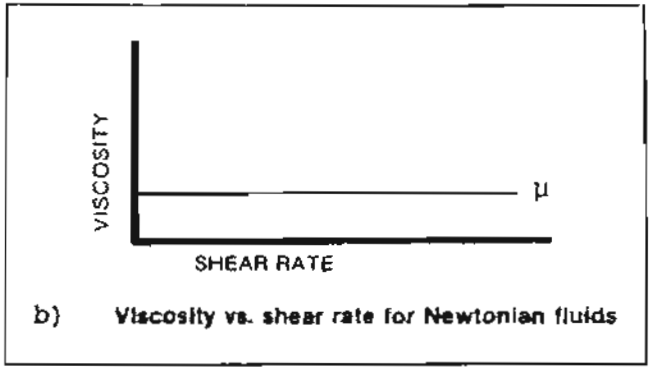


b) Viscosity vs. shear rate for Newtonian fluids

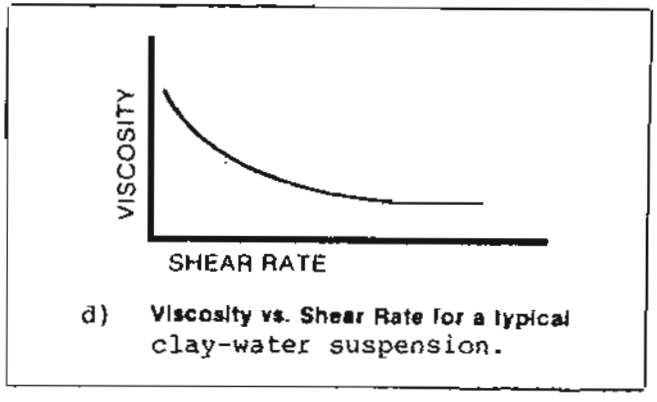


d) Viscosity vs. Shear Rate for a typical clay-water suspension.

Figure 8. Shear Stress vs. Shear Rate and viscosity vs. Shear Rate diagrams for Newtonian and non-Newtonian fluids[14].

sion. Two things in this rheogram are different from the one for a Newtonian fluid. First, the relationship is given by a curve instead of a straight line. Second, the fluid exhibits a yield stress; a certain amount of internal resistance must be overcome for the fluid to flow at all.

A Newtonian fluid has a constant viscosity that is inherent to the fluid at a fixed temperature. For instance, pure water has a viscosity of 1 centipoise at 20°C. However, a non-Newtonian fluid does not have a constant viscosity. Its viscosity depends on the rate at which it is sheared. Fig. 8d is a plot of viscosity versus shear rate for the suspension with the rheogram shown in Figure 8c. At any particular shear rate a fluid has a viscosity that is called the apparent viscosity ($\mu_a$) of the fluid at that shear rate. It is obvious that the apparent viscosity of a non-Newtonian fluid is dependent on the shear rate at which it is determined.

To determine exactly the rheogram for a Newtonian fluid, it is only necessary to know the shear stress at a single shear rate. That point then is plotted on rectangular coordinate paper, and a straight line is drawn through that point and the origin. To determine exactly the rheogram for a non-Newtonian fluid, it would be necessary to use an infinitely variable-speed viscometer.

Thus, in attempting to assess the effect of increasing viscosity due to increasing clay concentrations in recycled placer mining process water on the settling velocity of gold particles one must consider several points. First, the nature of the rheogram which describes the suspensions viscosity, i.e. does the suspension behave as a Newtonian as a non-Newtonian fluid.

If the fluid shows non-Newtonian behavior then it must be realized that its viscosity will vary depending upon the rate at which it is sheared. With respect to gold particles settling through a non- Newtonian suspension, this means that a large particle, with a high settling velocity, will be affected by a much different viscosity than a fine gold grain, which settles more slowly through the same suspension.

Finally, the fact that clay-water suspensions may display a yield stress intercept in their rheogram, emphasizes that there is a certain size (mass) below which no settling will occur. Hence, it seems highly desirable to define recycled placer process fluids with respect to their equilibrium levels of suspended solids and to describe the viscous properties of these suspensions.

In the course of the present study a Fann Viscometer (model 35A) was used to determine the suspensions' apparent viscosities at varying shear rates. Figure 9 shows a schematic of such a viscometer. The fluid to be tested is placed in a container and raised to submerge the rotating sleeve and the bob within it. The fluid in the annulus between the bob and the sleeve is sheared by the rotation of the sleeve. The outside layer of fluid moves at the same speed as the sleeve. Inner layers move more slowly. The innermost layer imparts a torque on the bob. The shear rate is related to the rotary speed of the sleeve. At a constant rotary speed the amount of torque imparted to the bob is governed by the resistance of the fluid.

The formula for apparent viscosity is:

$$\mu_a = 300 \frac{F}{R} \qquad \text{Eq. 17}$$

where R = Fann Viscometer rotary speed, rpm

F = Fann Viscometer dial reading at rotary speed R, lb/100 ft$^2$

$\mu_a$ = apparent viscosity at R in centipoise.

In assessing the impact of increases in fluid viscosity on the settling velocity of gold particles, Figure 1 and Eq. 13 are again helpful. In the Newtonian range Eq. 13 reduces to Eq. 3, in which no viscosity term appears. Hence, an increase in fluid viscosity in this settling regime should cause no decrease in a particles terminal settling velocity.

At the other end of the settling range, Stokes' settling, viscosity is inversely proportional to terminal settling velocity (Eq. 2). It follows then that a doubling in the fluid viscosity would cause a 50% decrease in settling velocity.

For transitional settling, viscosity enters equation 13 through the drag coefficient, $C_D$. $C_D$ is a function of the Reynolds number as shown in Figure 1. Since the Reynolds number is inversely proportional to the viscosity of the fluid (Eq. 2), an increase in fluid viscosity leads to a decrease in the Reynolds number. As Figure 1 shows, a decrease in the Reynolds number correlates to an increase in the drag coefficient, $C_D$, and hence a decrease in the terminal settling velocity.

## LABORATORY PROCEDURE AND EXPERIMENTAL DESIGN

### Settling Velocity Measurement System

Figure 10 shows a schematic of the settling velocity measurement system designed and used by MIRL during the course of the study. Shielded NaI (Tl) scintillators monitored the settling column through detection slits at heights $h_1$ and $h_2$. The distance between the detection slits is designated $\Delta h$. Water is fed to the base of the settling column

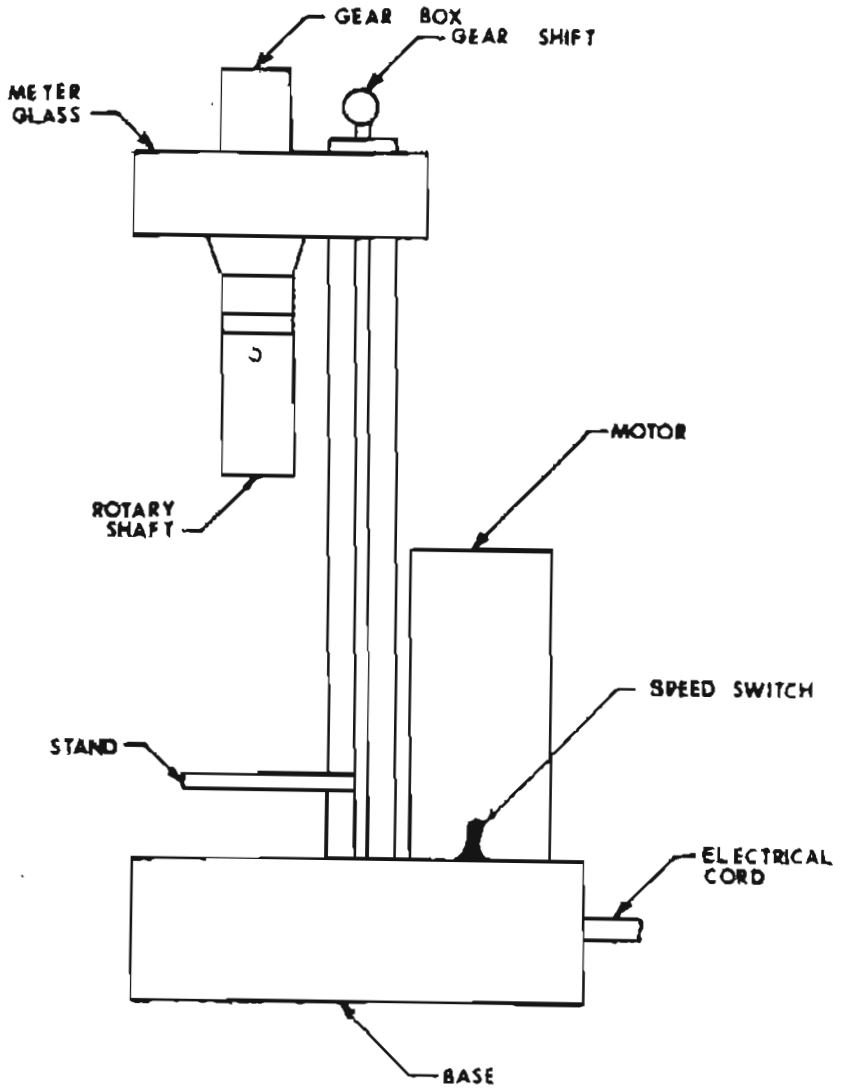


Figure 9. Schematic of Fann viscometer[16].

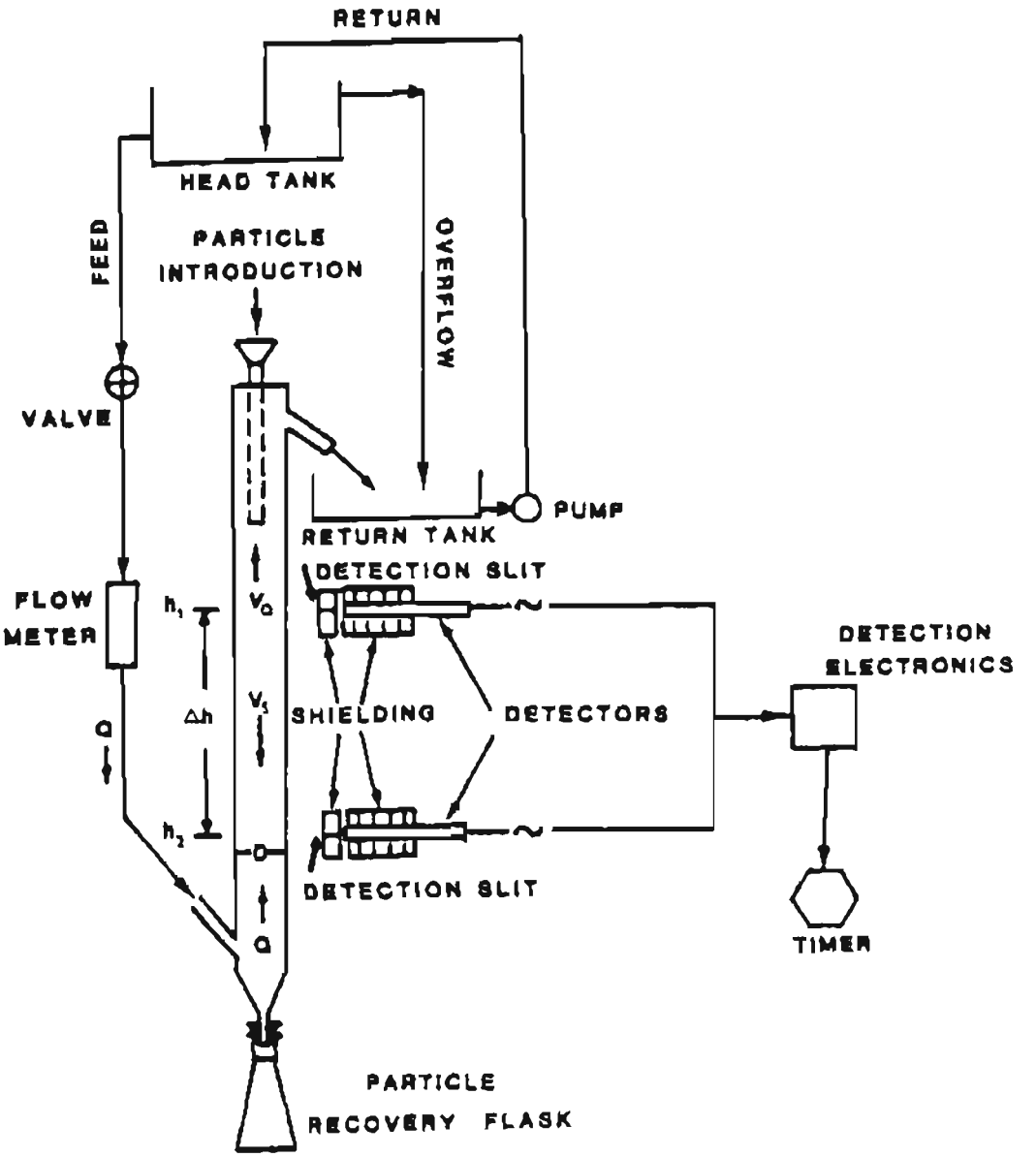


Figure 10. MIRL's settling velocity measurement system.

from a head tank at a flow rate, Q, which is measured by the circuit's flowmeter. Given the settling column with inside diameter, D, the upward flow velocity ($V_Q$) of the water is given by:

$$V_Q = 4(Q)/\pi D^2 \qquad \text{Eq. 18}$$

A neutron activated gold particle introduced through the funnel at the top of the settling column will reach its equilibrium settling velocity above $h_1$ and continue to settle passed the detectors, settling through the distance $\Delta h$ in time period t, obtained from the timer. The settling velocity of the gold particle is given by Equation 19.

$$\begin{aligned} V_S &= \Delta h/t + V_Q \\ &= \Delta h/t + 4(Q)/\pi D^2 \\ &= C_1/t + C_2(Q) \end{aligned} \qquad \text{Eq. 19}$$

$C_1$ and $C_2$ are system constants. $C_1$ equals the distance, $\Delta h$, between detectors and $C_2$ is equal to the quantity $4/\pi(D)^2$.

The system as developed by MIRL consisted of a 46.4 mm inside diameter glass tube of 183 cm length. The head tank was placed 305 cm above the base of the settling column. Fluid was cycled between the head tank and the return tank by means of a varistaltic pump. A Gilmont ball type flowmeter was used to monitor the fluid flowrates to the settling column. It was calibrated by weighing timed samples taken of each of the fluids used in the course of this project.

Neutron activated gold ($^{198}Au$) emitted 0.410 MeV gamma radiation which was detected by Canberra 51 cm x 51 cm NaI (Tl) scintillators and associated electronics. The start and stop detection pulses produced by the electronics controlled a frequency counter, which acted as the system's timer. The frequency counter was an Intersil kit with 8 place digital readout.

Prior to finalization of system design, an uncertainty analysis[13] of anticipated experimental results was run. The following system parameters were used to run the analysis:

a) System fluid flow rate (Q): 10 $cm^3/sec \pm 1$ $cm^3/sec$

b) Column inside diameter (d): 46.4 mm ± 0.1 mm

c) Measured settling distance ($\Delta h$): 121.9 cm ± 0.1 cm

d) Settling time (t): t ± 0.001 sec.

The settling time entered into the analysis was of course dependent upon the size and shape of the gold used. For preliminary estimates of the systems accuracy, Stokes' and Newtonian settling velocity equations were used to estimate the settling times for 37 micron diameter and 2.38 mm diameter particles respectively. Using these values the uncertainty analysis indicated that actual settling velocities measured by the system would be subject to less than a 1% error.

In order to determine at what distance from the water surface level at the top of the column to place the first scintillation detector, to assure that a particle reached its terminal settling velocity prior to starting the timer, a computer program was written. The program simulated the settling behavior of a 2.38 mm gold sphere, the most massive particle used in this study, taking into account the variable acceleration acting on the sphere over time. This program indicated that the sphere would reach 99.5% of its terminal velocity at a distance of 20.5 cm below the water surface. As the system was finally set up, the upper detector was positioned approximately 30 cm below the water level surface.

**Description of Gold Particles Used in the Study**

The gold particles used during the course of this project were of two types, (1) manufactured gold particles and (2) natural gold particles. The manufactured particles were used in order to:

1) Keep surface roughness and porosity to a minimum;

2) Maintain a constant density between gold particles;

3) Approach a spherical shape where required;

4) Approach a disc-like shape during flattening; and

5) Allow more accurate measurement of gold grains due to the absence of edge-roughness.

Natural gold grains were used to check how closely their settling behavior corresponded to the ideal case of their manufactured counterparts.

The manufactured grains were formed from -100 mesh (-149 microns) gold with a fineness of approximately 850. The gold was obtained from Del Ackels' mine located on Gold Dust Creek, Circle Mining District, Alaska. Gold particles of the following nominal sizes were manufactured for the study; 8 mesh (2.38 mm), 14 mesh (1.49 mm), 30 mesh (595 microns), 50 mesh (297 microns), 100 mesh (149 microns), 200 mesh (74 microns), 270 mesh (53 microns),

400 mesh (37 microns) 26 microns, 18 microns, and 15 microns. For the sizes 8 mesh through 400 mesh, four different particle shapes were made for each size. These shapes corresponded to Corey's Shape Factor values of 1.0 (spherical), 0.7, 0.3, and 0.1. For the three smallest size particles used, 26 microns through 15 microns, only a single spherical particle was manufactured. Table 2 gives the descriptive data of each of the manufactured gold grains.

As a practical guide to the sizes and shapes of gold studied in this project, the authors relied primarily upon personal experience with Alaskan gold and the previous gold settling velocity work done by Shilo and Shumilov[4]. It can be seen from Figure 6 that the majority of natural gold studied by the Soviet scientists fell into a flatness factor range of from 1 to 10, corresponding to a Corey's shape factor range of 1 to 0.1. A predominance of Alaskan gold also falls in this range, with the exception of some marine placers which possess Corey's shape factors below 0.1.

With respect to the size of gold studied, the authors wished to extend the work of previous researchers well below the 2 mg limit, but work with large enough particles to overlap settling velocity data available in the literature. From previous work with the radiotracer $^{198}Au$, in evaluating gold concentration by compound water cyclones, the authors were given confidence that they could accurately detect extremely fine gold grains, i.e. 400 mesh (37 microns) and perhaps finer. A practical lower size limit was imposed more from the technical realities of handling, measuring, and shaping the particles, than from their detection.

The particles were made using one of two techniques depending upon the size of the grain. For particles of 100 mesh size and larger, a calculated gold mass was weighed out and wrapped in lead foil, then fired in a bone ash cupel. The resulting spherical grain was removed, rinsed clean with acetic acid and distilled water and stored. Grains which required a final spherical shape (CSF = 1.0) were measured using either a dial caliper (± 0.02 mm), for 8 mesh and 14 mesh grains, or a Leitz Ortholux ore microscope, fitted with a Leitz Vickers hardness tester micrometer eyepiece (± 2 micron), for 30 mesh to 100 mesh particles. Grains requiring a Corey's shape factor of less than unity were flattened in an Infra Red pellet press using machinist thickness gauges as a press stops.

The process of forming particles of less than 100 mesh size began by sprinkling natural gold grains of an appropriate size range into a lithium metaborate flux and firing them in a graphite crucible. The resulting molten mass was poured hot into a porcelain crucible containing a 10% $HNO_3$ solution. After the flux was dissolved by the acidic solution, spherical gold grains remained. The resultant particles were observed under a binocular microscope to locate particles of approximately the correct size. These chosen particles were then measured more precisely using the Leitz Ortholux microscope. Grains which required flattening were pressed using a machinist depth micrometer and anvil arrangement designed by the authors. The process of forming the grains finer than 200 mesh was tedious and time consuming. Approximately 2 to 4 hours were required to fabricate each of these fine grains.

It will be noted from Table 2 that the mass of each particle is listed. Those values not marked with an asterisk (*) are actual weighed values. A Perkin-Elmer TGS-2 balance from a thermogravimetric analysis system was used to weigh the gold grains to ± 0.1 microgram accuracy. The calculated gold masses of Table 2, those values marked with an asterisk, were derived from volume calculations of the measured grains and the average gold density obtained from the direct weighing of the larger particles.

Three sizes of natural gold particles with two shape factors per size (a total of six size-shape combinations) were sorted for the project. These were 14 mesh (1.41 mm), 50 mesh (297 micron), and 100 mesh (149 micron) nominal size grains with Corey's shape factors of 0.7 and 0.1 for the 14 mesh gold and 0.7 and 0.3 for the other two sizes.

The process of sorting the gold took place in three steps. Grains were visually observed to choose those particles with regular shape, rejecting those with highly porous surfaces, unusually rough edges, or highly irregular form. Disc like shapes were the guide for particle choice. The conforming grains were then measured; the 14 mesh particles using a dial caliper and the finer grains using the Ortholux microscope. Any particle which had an average projected surface dimension ($\sqrt{ab}$) of nominal size ± 10% nominal size was noted for subsequent thickness measurement. Other grains not meeting this criteria were discarded. After thickness measurements were completed, a Corey's shape factor was calculated for each grain. If the calculated shape factor fell within the range of nominal shape factor ± 0.05, the particle was accepted for future test work, otherwise it was rejected. Between 30 and 40 grains for each natural size-shape combination were collected.

Both manufactured and natural grains which were chosen as acceptable, were stored in individually labeled 0.4 dram polyethylene vials or pure quartz glass vials depending upon which nuclear reactor was receiving them. The grains were neutron activated for a specified period of time to yield an initial activity of approximately $1 \times 10^6$ disintegrations per second (dps). This activity allowed for 2 to 3 weeks of useful working life in the laboratory. The half life of $^{198}Au$ is 2.7 days.

Table 2
Characteristics of Manufactured Gold Particles
Used in Phase One

| Nominal Particle Description ASTM Mesh (microns) | Measured Particle Dimensions (microns unless otherwise labeled) a | b | c | Corey's Shape Factor ($c/\sqrt{ab}$) | Particle Mass (micrograms unless otherwise labeled) |
|---|---|---|---|---|---|
| | 2.40mm | 2.40mm | 2.40mm | 1.0 | 96.96mg |
| 8 | 2.50mm | 2.50mm | 1.60mm | 0.64 | 101.26mg |
| (2380) | 2.50mm | 2.13mm | 0.68mm | 0.29 | 44.55mg |
| | 2.26mm | 2.04mm | 0.24mm | 0.11 | 15.18mg |
| | 1.38mm | 1.38mm | 1.38mm | 1.0 | 23.60mg |
| 14 | 1.36mm | 1.36mm | 1.02mm | 0.75 | 21.04mg |
| (1410) | 1.38mm | 1.38mm | 0.39mm | 0.38 | 8.89mg |
| | 1.36mm | 1.36mm | 0.11mm | 0.08 | 2.51mg |
| | 590 | 590 | 590 | 1.0 | 1.87mg |
| 30 | 590 | 590 | 460 | 0.68 | 1.44mg |
| (595) | 650 | 580 | 185 | 0.30 | 887.0 |
| | 625 | 550 | 50 | 0.08 | 187.0 |
| | 312 | 312 | 312 | 1.0 | 269.0 |
| 50 | 312 | 312 | 240 | 0.77 | 241.0 |
| (297) | 300 | 300 | 80 | 0.27 | 110.0 |
| | 312 | 312 | 30 | 0.10 | 38.0 |
| | 162 | 162 | 162 | 1.0 | 31.0 |
| 100 | 152 | 152 | 108 | 0.71 | 25.0 |
| (149) | 155 | 155 | 50 | 0.32 | 14.0 |
| | 175 | 112 | 15 | 0.11 | 3.2 |
| | 75 | 75 | 75 | 1.0 | 3.7 |
| 200 | 88 | 68 | 55 | 0.72 | 3.5 |
| (74) | 75 | 80 | 20 | 0.26 | 1.7* |
| | 74 | 71 | 7 | 0.10 | 0.5* |
| | 52 | 52 | 52 | 1.0 | 1.1 |
| 270 | 52 | 52 | 33 | 0.63 | 0.8 |
| (53) | 44 | 60 | 16 | 0.31 | 0.6* |
| | 45 | 72 | 9 | 0.16 | 0.4* |
| | 40 | 40 | 40 | 1.0 | 0.6* |
| 400 | 42 | 42 | 29 | 0.69 | 0.7* |
| (37) | 34 | 34 | 11 | 0.32 | 0.2* |
| | 34 | 34 | 3 | 0.09 | 0.05* |
| (26) | 26 | 26 | 26 | 1.0 | 0.16* |
| (18) | 18 | 18 | 18 | 1.0 | 0.05* |
| (15) | 15 | 15 | 15 | 1.0 | 0.03* |

**Experimental Phases of the Study**

The original experimental design of the laboratory test work of this project was broken down into the four phases listed below:

Phase 1. The settling velocities for the 35 manufactured gold particles would be determined. The goal of this phase of the study was to produce working gold settling velocity vs. size-shape graphs for practical engineering application.

Phase 2. Gold spheres would be progressively flattened through 3 stages. At each flatness stage their settling velocity would be determined. This phase would highlight the effect on settling velocity of decreasing shape factor for particles of constant mass.

Phase 3. The settling velocity of natural gold particles would be determined. This phase would allow the settling velocities of natural particles to be compared to those of the corresponding manufactured particles. Inferences could be drawn concerning settling velocity discrepancies, if any.

Phase 4. A generalized randomized block design would be generated to explore the effects of three variables on the settling velocity of gold grains. The design was to be blocked according to gold size-shape combinations. The three variables (factors) to be studied were water temperature, clay concentration in the fluid, and the clay mineralogy of the suspended clays.

Each of these phases is discussed below in detail.

*Phase 1*

Each of the 35 manufactured gold particles was randomly selected and processed through the settling velocity measurement system (Figure 10) eleven times. After completing all 35 particles, the process was repeated, using a new random order. This process was repeated a third time, after which each particle had 33 recorded settling times. It was desirable to make at least 30 observations of settling times for each particle in order to obtain an accurate estimate of settling velocity variance per particle. The three extra observations per particle allowed for discarding outlier values if they were present. The estimate of settling velocity variance per particle would be useful in planning phase 4 of the study, i.e. the generalized block design.

All of these settling velocity measurements were made in clear, ambient temperature water with no induced upward velocity in the settling column, though thermal currents were perhaps present. The actual fluid temperature was recorded during each series of eleven settling times. Using the measured distance of fall (to the nearest millimeter) and the settling times, settling velocities were calculated for all particles.

From the variance of the settling velocities, the number of observations, and the mean settling velocities, confidence interval estimates of the true mean settling velocity for each particle were tabulated. The data was presented graphically for ready use by the gold processing industry.

*Phase 2*

In order to evaluate the effect of shape on a particles settling velocity for gold grains of constant mass, eight of the spherical particles (8 mesh through 400 mesh) used in phase 1 were progressively flattened. The degrees of flatness were chosen in advance at 1.0 (phase 1 values), 0.5, 0.1, and 0.05. Particles, depending upon their size, were flattened by one of the two methods previously described. Table 3 shows the dimensions of these particles.

It was originally planned to make 33 observations of settling velocity at each degree of flatness for each particle. However, after the completion of phase 1 showed such low standard deviations about mean settling velocity values (<5% of the mean value) it was decided to limit the number of observations to eleven per degree of flatness per particle. Again, the order of observations was randomized. Results were both tabulated and plotted in graphical form. As in phase 1, these settling velocity measurements were observed in clear, ambient temperature water with no upward velocity.

*Phase 3*

Initially it was planned to determine settling velocities for six size-shape combinations of natural gold particles, i.e. 14 mesh (0.7 and 0.1), 50 mesh (0.7 and 0.3) and 100 mesh (0.7 and 0.3). However, due to a delay in the gold's shipment after neutron activation, the 100 mesh gold was no longer active enough for laboratory use after arrival. Because of the additional expense of another activation and the scheduling of the project, the 100 mesh gold was dropped from the design.

For each of the four remaining particle classifications there were at least 30 grains of gold per grouping. Settling velocities were determined in clear, ambient temperature water with no upward velocity. Each grain was passed through the system only once. A mean settling velocity for a size-shape combination was determined by averaging the settling velocities for the individual grains of that grouping. These mean values were tabulated and compared to those settling velocities of the manufactured gold grains.

*Phase 4*

Of primary interest to this project was the study of the

Table 3
Characteristics of Manufactured Gold Particles
Used in Phase 2

| Mass of Particle | Measured Particle Dimensions (microns unless otherwise labeled) a | b | c | Corey's Shape Factor ($c/\sqrt{ab}$) | Nominal CSF |
|---|---|---|---|---|---|
| | 2.40mm | 2.40mm | 2.40mm | 1.0 | 1.0 |
| 97.0 mg | 2.52mm | 2.45mm | 1.48mm | 0.6 | 0.5 |
| (8 mesh | 3.90mm | 3.74mm | 0.46mm | 0.1 | 0.1 |
| sphere) | 5.10mm | 4.50mm | 0.30mm | 0.06 | 0.05 |
| | 1.38mm | 1.38mm | 1.38mm | 1.0 | 1.0 |
| 23.6 mg | 1.60mm | 1.44mm | 0.92mm | 0.6 | 0.5 |
| (14 mesh | 2.92mm | 2.12mm | 0.26mm | 0.1 | 0.1 |
| sphere) | 3.50mm | 2.68mm | 0.17mm | 0.05 | 0.05 |
| | 590 | 590 | 590 | 1.0 | 1.0 |
| 1.9 mg | 700 | 620 | 360 | 0.5 | 0.5 |
| (30 mesh | 1140 | 1060 | 100 | 0.09 | 0.1 |
| sphere) | 1560 | 1360 | 75 | 0.05 | 0.05 |
| | 312 | 312 | 312 | 1.0 | 1.0 |
| 0.3 mg | 360 | 340 | 200 | 0.6 | 0.5 |
| (50 mesh | 630 | 495 | 70 | 0.1 | 0.1 |
| sphere) | 730 | 675 | 35 | 0.05 | 0.05 |
| | 162 | 162 | 162 | 1.0 | 1.0 |
| 31.0 µg | 162 | 162 | 92 | 0.6 | 0.5 |
| (100 mesh | 395 | 330 | 25 | 0.07 | 0.1 |
| sphere) | 450 | 370 | 20 | 0.05 | 0.05 |
| | 75 | 75 | 75 | 1.0 | 1.0 |
| 3.7 µg | 85 | 80 | 42 | 0.5 | 0.5 |
| (200 mesh | 145 | 140 | 14 | 0.1 | 0.1 |
| sphere) | 225 | 210 | 9 | 0.04 | 0.05 |
| | 52 | 52 | 52 | 1.0 | 1.0 |
| 1.1 µg | 75 | 58 | 20 | 0.4 | 0.5 |
| (270 mesh | 145 | 100 | 10 | 0.08 | 0.1 |
| sphere) | – | – | – | – | – |
| | 40 | 40 | 40 | 1.0 | 1.0 |
| 0.6 µg | 45 | 40 | 23 | 0.5 | 0.5 |
| (400 mesh | 90 | 80 | 9 | 0.08 | 0.1 |
| sphere) | – | – | – | – | – |

effects of suspended clays on the settling velocity of gold particles. In order to attempt to definitively describe these effects a generalized randomized block design was employed with particle size-shape combinations as the blocking variable. There were a total of eight blocks. These consisted of four manufactured particles (14 mesh (0.7 and 0.1) and 50 mesh (0.7 and 0.3)) and four natural particle groups of 10 particles each (14 mesh (0.7 and 0.1) and 50 mesh (0.7 and 0.3)). As in phase 3, it was originally planned to include 100 mesh gold in this factorial design, but it was dropped due to an extended delivery time.

Three factors, in addition to the blocking variable, were included in the design. These were:

1) Two factor levels of the mineralogy of the suspended clays, i.e. Georgia Kaolin and Wyoming Bentonite.

2) Four factor levels of suspended clay concentration. The nominal concentration levels targeted for study were 0 g/l (clear water), 10 g/l, 25 g/l and 50 g/l. In laboratory practice however, because of some settling in the head and return tanks and screening the clay-water suspension at 400 mesh (37 microns) prior to using it in the settling velocity measurement system, the actual clay concentrations during the test were approximately 20% less than the planned levels.

3) Two temperature factor levels were studied; ambient temperature, which varied from 18°C to 22°C and a cold temperature which ranged from 3°C to 10°C. The cold temperature treatment levels were achieved by placing ice baths about the head and return tanks and using cold water (2°C) to make up the clay-water suspension.

This design consisted of 16 treatment levels (2 x 2 x 4) all of which were assigned to each of the eight blocks. The factorial design was randomized to an extent which still allowed it to remain practical to run in a timely fashion. This randomization consisted of the following steps:

1) A clay mineralogy was selected at random.

2) A temperature level was selected at random.

3) With the previous two factor levels set, the four clay concentrations were randomly assigned.

4) Within each of the 16 treatments, the blocks were randomly assigned position. A single replication (n=2) was run sequential to the initial settling velocity observations of the eight size-shape combinations (blocks).

Hence, once a clay mineralogy-temperature level had been assigned all clay concentration and block levels, with replication, were run prior to moving on to the next clay mineralogy-temperature level. This practice kept clean-up time between clay types to a minimum and allowed the system to remain at a low temperature during a cold temperature factor level.

The design of the settling velocity measurement system allowed for rapid circulation of slurry between the head tank and the return tank in order to help keep the minus 37 micron material in suspension. When suspensions of kaolin were being run, an upward flowrate of approximately 525 ml/min was maintained in the settling column. Where bentonitic suspensions were used an upward flowrate of 150 to 550 ml/min was maintained for 14 mesh particles. However, due to the slowing effect bentonite-water suspension exhibited on 50 mesh particles, the upward flow rate was completely eliminated in order to allow more timely testing. In such cases, the system was frequently circulated in the absence of gold particles, to assure good mixing of the slurry and even temperatures.

During the tests, 200 ml samples of the clay-water suspension were taken at three times for each clay mineralogy-temperature- concentration level. The first sample was taken prior to settling any particles, but after the system had circulated for some time. A second fluid sample was taken between replications and a final sample was collected at the completion of the concentration level. This yielded a total of 36 samples (12 levels x 3 samples).

For each sample, turbidity and total suspended solids were determined. The temperature of the fluid was recorded during the settling of each particle group. Later, after the suspended solids levels of the suspensions had been analyzed, suspensions with average suspended solid levels of grouped samples were made up, and their viscosities measured at the appropriate temperature.

Where a block consisted of natural gold grains, 10 grains were used. Each was allowed to settle one time per replication. Thus, for natural particles, a replicate data value consisted of the mean of 10 settling velocities. For those blocks of manufactured particles, a single particle was settled 5 times per replication. These five settling velocities were averaged.

After phase 1 had been completed and the data analyzed it was obvious that while the variance, as a percent of the mean settling velocity, was fairly constant between gold size-shape combinations, it was highly variable between gold size-shape combinations on a velocity units squared ($cm^2/sec^2$) basis. Since a fixed effects analysis of variance (ANOVA), model was being used and treatment sample

sizes were all equal (n = 2) it was felt that heteroscedacity (nonconstant variance) posed no serious problem for the comparison of factor affects. However, heteroscedacity could prove a problem in contrast comparisons for data resulting from the randomized block design. This suggested that contrast comparisons should quite probably be confined within a block. Later, this became a rather mute point, since, as will be seen in the next chapter, the highly significant interaction effects present among the factors, dictate within block contrast comparison at the very least.

Regarding multiple comparison techniques, prior to the completion of the experiment it was not known by the authors which comparison of factor effects would be of interest, excepting of course the initial multiple comparison to determine which factors and interactions were significant. For this reason, the Tukey method should be used to maintain an experiment wise error rate for any family of comparisons made after concluding significant factor or interaction effects. The Bonferroni method of multiple comparisons was used to maintain a family significance level for the initial joint statement concerning factor and interaction effects, since this testing process did not involve "data snooping".

After the experiment was completed, the data was entered into the University of Alaska's Vax computer system and analyzed using SAS, SPSS, and MINITAB software. DISPLA software was used for graphic presentation of the data.

## EXPERIMENTAL RESULTS

**Phase 1**

The settling velocities for the 35 manufactured gold particles were determined. The goal of this phase of the study was to produce gold settling velocity vs. size-shape tables and graphs for practical engineering application.

Table 4 presents the results of phase 1. Both individual and family confidence intervals are given for the mean settling velocities for a level of significance, $\alpha$, equal to 0.05. Figures 11 and 12 show plots of the mean settling velocities versus gold size and shape using two different scales; i.e. log and log-log scales respectively.

**Phase 2**

Gold spheres were progressively flattened through 3 stages. At each flatness stage their settling velocity was determined in order to study the effect on settling velocity of decreasing shape factor for particles of constant mass. The results of phase 2 are presented in Table 5. As in phase 1, both individual and family confidence intervals for the mean settling velocities are shown for $\alpha$ equals 0.05. Figures 13 and 14 graphically display the data of Table 5. Note that settling velocity values for 1.1 μg x 0.05 CSF and 0.6 μg x 0.05 CSF particles are absent. These values were not obtained. During the flattening process these very fine gold particles were destroyed; i.e. fragmented.

**Phase 3**

The settling velocities for 4 different size-shape combinations of natural gold particles were determined. This phase allowed the settling velocities of natural particles to be compared to those of the corresponding manufactured particles.

Table 6 shows the results of phase 3. In each case, 30 natural gold particles were settled and timed. The average mass of each 30 particles is also given, as well as the 95% confidence interval for the mean settling velocity of each size-shape group.

Table 7 compares the mean settling velocities of natural and manufactured gold particles of the same size-shape combination. It appears that the difference in particle mass between natural and manufactured grains of the same size-shape group is primarily responsible for variations between their settling velocities.

**Phase 4**

An ANOVA of the generalized randomized block design was run to explore the effects of three variables on the settling velocity of gold grains. The design was blocked according to gold size-shape combinations. The three variables (factors) studied were water temperature, clay concentration in the fluid, and the clay mineralogy of the suspended clays.

Table 8 shows the results of the ANOVA. Note that all of the main effects (variables) are highly significant. As expected, the blocks accounted for a very large percentage of the main effects variance, hence the rationale for the employed blocking scheme. The remainder of the main effects variance is accounted for, in decreasing order of importance by clay mineralogy, clay concentration, and temperature.

All two way interactions are highly significant ($p < 0.001$) except for the non-significant temperature-clay mineralogy interaction. Three of the four three-way interactions are highly significant, the temperature-clay mineralogy-clay concentration interaction being non-significant. The four way interaction was also non-significant. All significance tests were made using a level of significance of $\alpha = 0.05$ and employing the Bonferroni technique for multiple comparisons.

A Bartlett test for constant variance among treatments was run, yielding a highly significant F test, $p < 0.001$. Thus

Table 4
Settling Velocities of Manufactured Gold Particles

| Nominal Gold Size (ASTM Mesh) | Nominal Gold Shape (CSF) | Number of Observations (n) | 95% Confidence Interval* of mean Settling Velocity (cm/sec) | 95% Family Confidence Interval** of mean Settling Velocity (cm/sec) |
|---|---|---|---|---|
| | 1.0 | 33 | 93.8 ± 1.2 | 93.8 ± 2.2 |
| 8 | 0.7 | 33 | 90.9 ± 1.1 | 90.9 ± 2.0 |
| | 0.3 | 33 | 51.8 ± 0.6 | 51.8 ± 1.0 |
| | 0.1 | 33 | 25.5 ± 0.2 | 25.5 ± 0.3 |
| | 1.0 | 33 | 76.4 ± 0.8 | 76.4 ± 1.5 |
| 14 | 0.7 | 33 | 68.8 ± 0.5 | 68.8 ± 0.9 |
| | 0.3 | 33 | 37.8 ± 0.4 | 37.8 ± 0.8 |
| | 0.1 | 33 | 17.3 ± 0.1 | 17.3 ± 0.2 |
| | 1.0 | 33 | 39.6 ± 0.2 | 39.6 ± 0.4 |
| 30 | 0.7 | 33 | 34.0 ± 0.1 | 34.0 ± 0.2 |
| | 0.3 | 33 | 22.7 ± 0.05 | 22.7 ± 0.1 |
| | 0.1 | 33 | 8.0 ± 0.02 | 8.0 ± 0.04 |
| | 1.0 | 33 | 20.5 ± 0.07 | 20.5 ± 0.13 |
| 50 | 0.7 | 33 | 19.7 ± 0.05 | 19.7 ± 0.09 |
| | 0.3 | 33 | 10.8 ± 0.06 | 10.8 ± 0.10 |
| | 0.1 | 33 | 4.9 ± 0.01 | 4.9 ± 0.02 |
| | 1.0 | 33 | 9.0 ± 0.02 | 9.0 ± 0.04 |
| 100 | 0.7 | 33 | 8.0 ± 0.04 | 8.0 ± 0.07 |
| | 0.3 | 33 | 5.5 ± 0.04 | 5.5 ± 0.07 |
| | 0.1 | 33 | 2.0 ± 0.02 | 2.0 ± 0.03 |
| | 1.0 | 33 | 3.94 ± 0.02 | 3.94 ± 0.04 |
| 200 | 0.7 | 33 | 3.25 ± 0.02 | 3.25 ± 0.04 |
| | 0.3 | 33 | 1.68 ± 0.02 | 1.68 ± 0.03 |
| | 0.1 | 33 | 0.71 ± 0.01 | 0.71 ± 0.02 |
| | 1.0 | 33 | 2.29 ± 0.03 | 2.29 ± 0.06 |
| 270 | 0.7 | 33 | 1.65 ± 0.02 | 1.65 ± 0.03 |
| | 0.3 | 33 | 1.19 ± 0.03 | 1.19 ± 0.05 |
| | 0.1 | 33 | 0.69 ± 0.02 | 0.69 ± 0.03 |
| | 1.0 | 33 | 1.35 ± 0.03 | 1.35 ± 0.05 |
| 400 | 0.7 | 33 | 1.32 ± 0.02 | 1.32 ± 0.04 |
| | 0.3 | 33 | 0.53 ± 0.01 | 0.53 ± 0.02 |
| | 0.1 | 33 | 0.16 ± 0.006 | 0.16 ± 0.01 |
| 26 µm | 1.0 | 11 | 0.67 ± 0.05 | 0.67 ± 0.10 |
| 18 µm | 1.0 | 11 | 0.45 ± 0.02 | 0.45 ± 0.03 |
| 15 µm | 1.0 | 11 | 0.23 ± 0.01 | 0.23 ± 0.02 |

* $\alpha = 0.05$ $t(\alpha/2, 32) = 2.04$; $t(\alpha/2, 10) = 2.23$

** $\alpha = 0.05$ $t(\alpha/2(35), 32) = 3.61$; $t(\alpha/2(35), 10) = 4.58$

NOTE: For a more detailed description of particle size and shape seen Table 2.

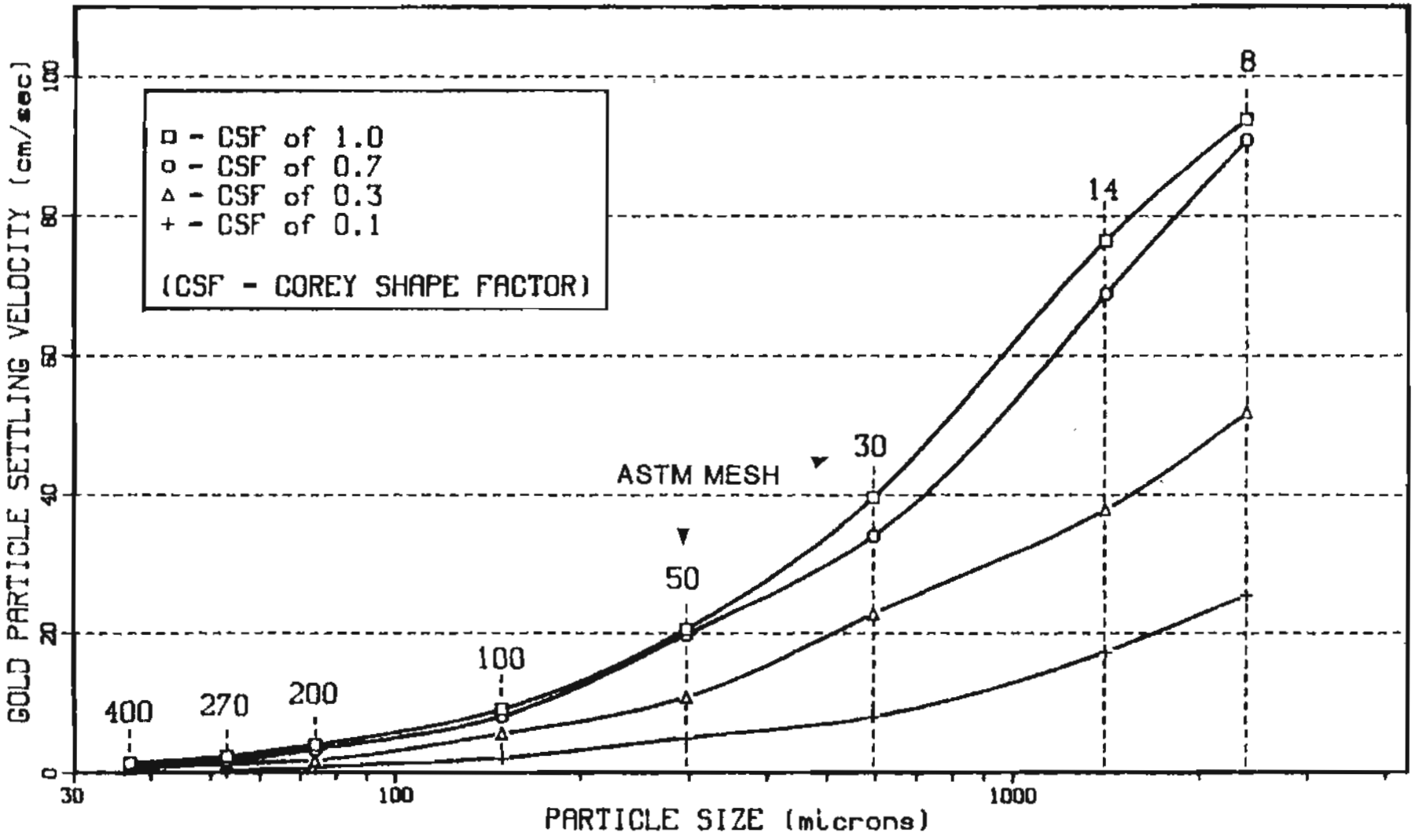


Figure 11. Settling velocities for gold particles of various sizes and flatnesses (semi-log scale).

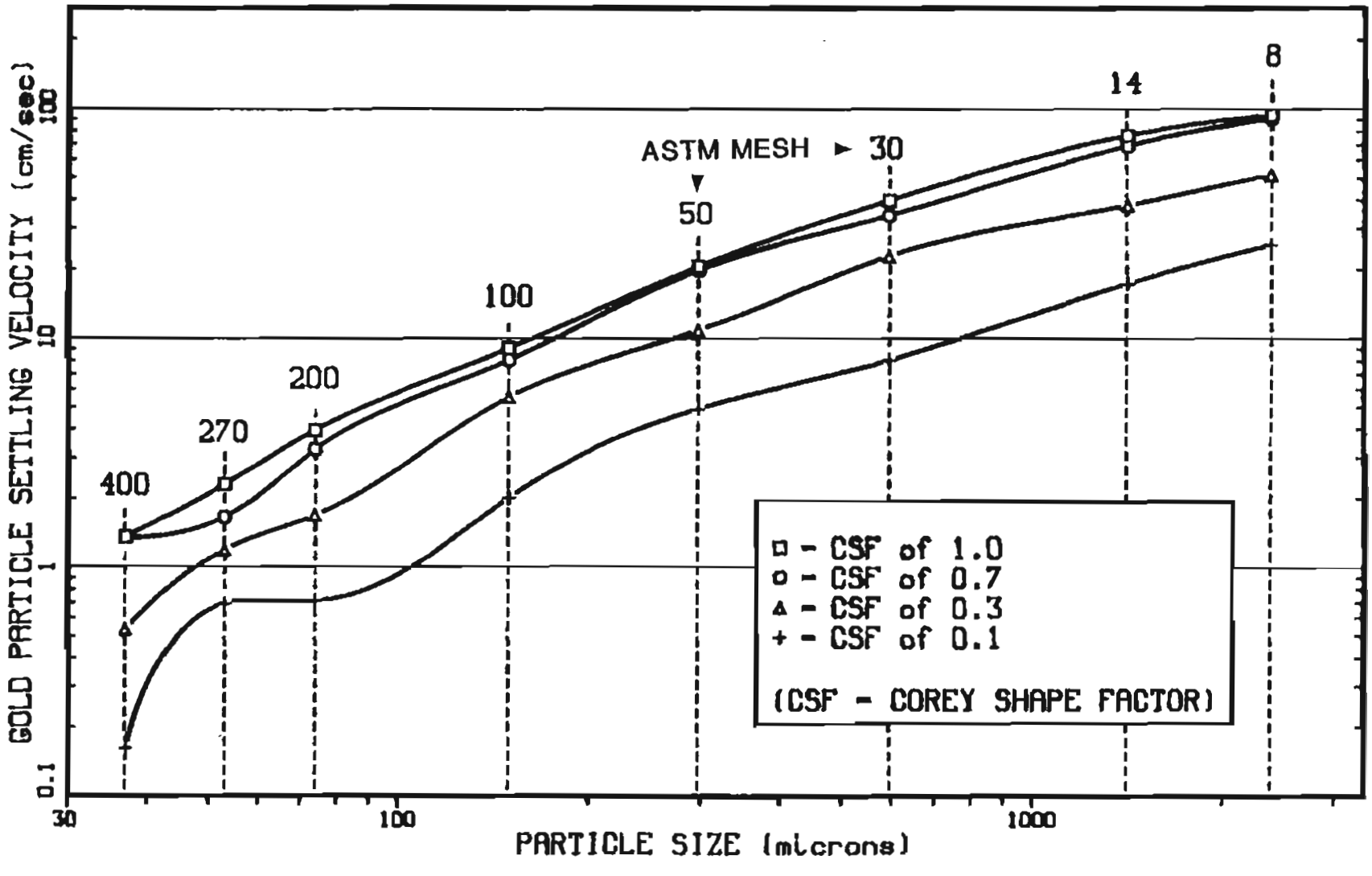


Figure 12. Settling velocities for gold particles of various sizes and flatnesses (log-log scale).

Table 5
Settling Velocities of Gold Particles of Constant Mass
at Various Flatnesses

| Gold Mass | Nominal Gold Shape (CSF) | Number of Observations (n) | 95% Confidence Interval* of mean Settling Velocity (cm/sec) | 95% Family Confidence Interval** of mean Settling Velocity (cm/sec) |
|---|---|---|---|---|
| | 1.0 | 33 | 93.8 ± 1.2 | 93.8 ± 2.2 |
| 97.0 mg | 0.5 | 11 | 85.3 ± 2.5 | 85.3 ± 5.2 |
| (8 mesh | 0.1 | 11 | 36.3 ± 0.8 | 36.3 ± 1.7 |
| sphere) | 0.05 | 11 | 26.2 ± 0.5 | 26.2 ± 1.0 |
| | 1.0 | 33 | 76.4 ± 0.8 | 76.4 ± 1.5 |
| 23.6 mg | 0.5 | 11 | 65.2 ± 0.7 | 65.2 ± 1.4 |
| (14 mesh | 0.1 | 11 | 26.7 ± 0.7 | 26.7 ± 1.4 |
| sphere) | 0.05 | 11 | 21.0 ± 0.3 | 21.0 ± 0.7 |
| | 1.0 | 33 | 39.6 ± 0.2 | 39.6 ± 0.4 |
| 1.9 mg | 0.5 | 11 | 34.8 ± 0.3 | 34.8 ± 0.6 |
| (30 mesh | 0.1 | 11 | 16.5 ± 0.2 | 16.5 ± 0.3 |
| sphere) | 0.05 | 11 | 13.7 ± 0.2 | 13.7 ± 0.3 |
| | 1.0 | 33 | 20.5 ± 0.07 | 20.5 ± 0.13 |
| 0.3 mg | 0.5 | 11 | 19.3 ± 0.06 | 19.3 ± 0.12 |
| (50 mesh | 0.1 | 11 | 10.8 ± 0.03 | 10.8 ± 0.07 |
| sphere) | 0.05 | 11 | 8.7 ± 0.03 | 8.7 ± 0.07 |
| | 1.0 | 33 | 9.0 ± 0.02 | 9.0 ± 0.04 |
| 31.0 µg | 0.5 | 11 | 8.4 ± 0.27 | 8.4 ± 0.57 |
| (100 mesh | 0.1 | 11 | 4.1 ± 0.07 | 4.1 ± 0.14 |
| sphere) | 0.05 | 11 | 3.6 ± 0.08 | 3.6 ± 0.16 |
| | 1.0 | 33 | 3.94 ± 0.02 | 3.94 ± 0.04 |
| 3.7 µg | 0.5 | 11 | 3.68 ± 0.10 | 3.68 ± 0.14 |
| (200 mesh | 0.1 | 11 | 2.29 ± 0.04 | 2.29 ± 0.09 |
| sphere) | 0.05 | 11 | 1.56 ± 0.05 | 1.56 ± 0.09 |
| | 1.0 | 33 | 2.29 ± 0.03 | 2.29 ± 0.06 |
| 1.1 µg | 0.5 | 11 | 2.05 ± 0.03 | 2.05 ± 0.07 |
| (270 mesh | 0.01 | 11 | 1.19 ± 0.02 | 1.19 ± 0.04 |
| sphere) | 0.05 | – | — | — |
| | 1.0 | 33 | 1.35 ± 0.03 | 1.35 ± 0.05 |
| 0.6 µg | 0.5 | 11 | 1.25 ± 0.04 | 1.25 ± 0.08 |
| (400 mesh | 0.1 | 11 | 0.78 ± 0.01 | 0.78 ± 0.03 |
| sphere) | 0.05 | – | — | — |

* $\alpha = 0.05$ $t(\alpha/2, 32) = 2.04$; $t(\alpha/2, 10) = 2.23$
** $\alpha = 0.05$ $t(\alpha/2(30), 32) = 3.60$; $t(\alpha/2(30), 10) = 4.58$

NOTE: For a more detailed description of particle size and shape see Table 3.

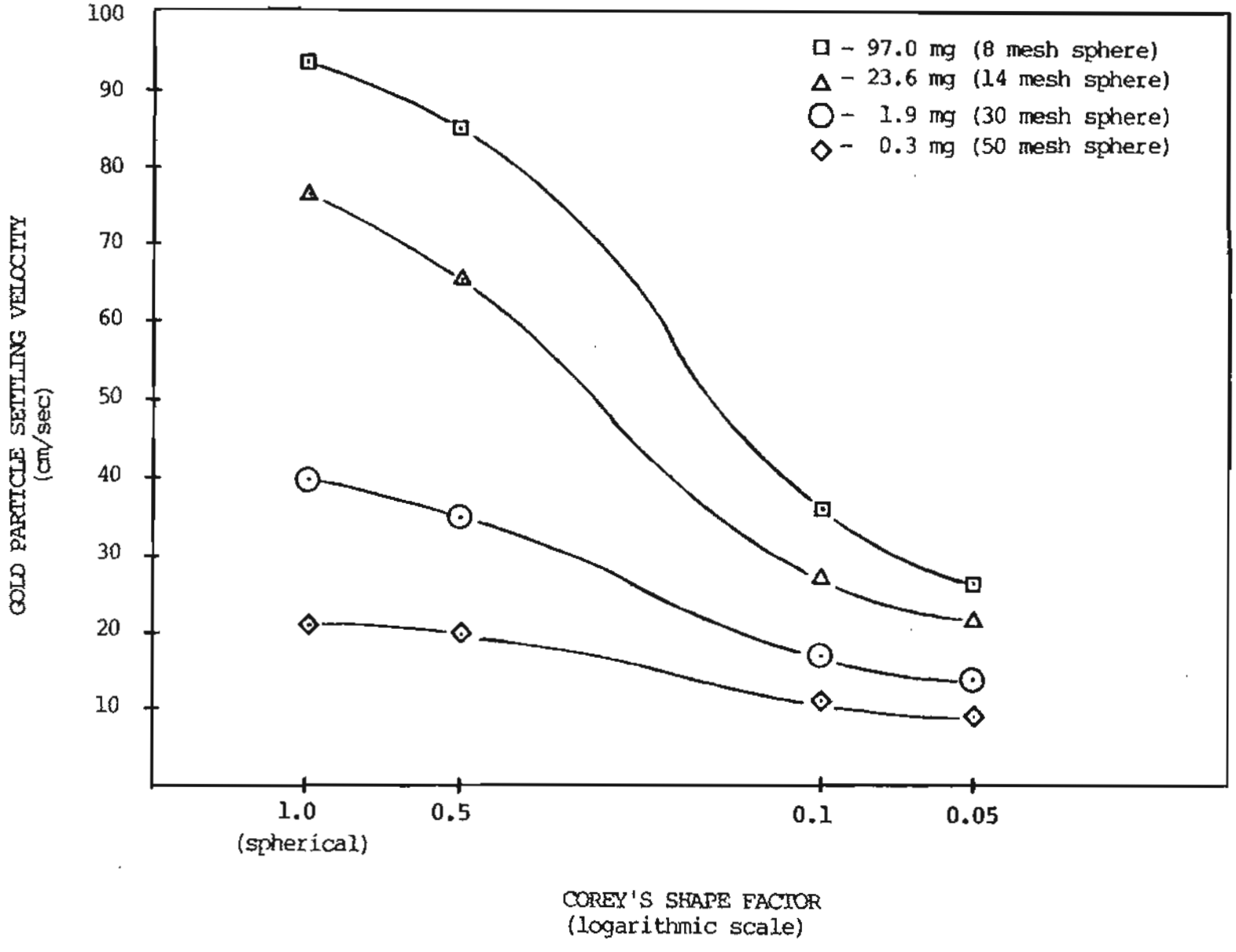


Figure 13. Settling velocities for gold particles of constant mass at various flatnesses (97 mg to 0.3 mg).

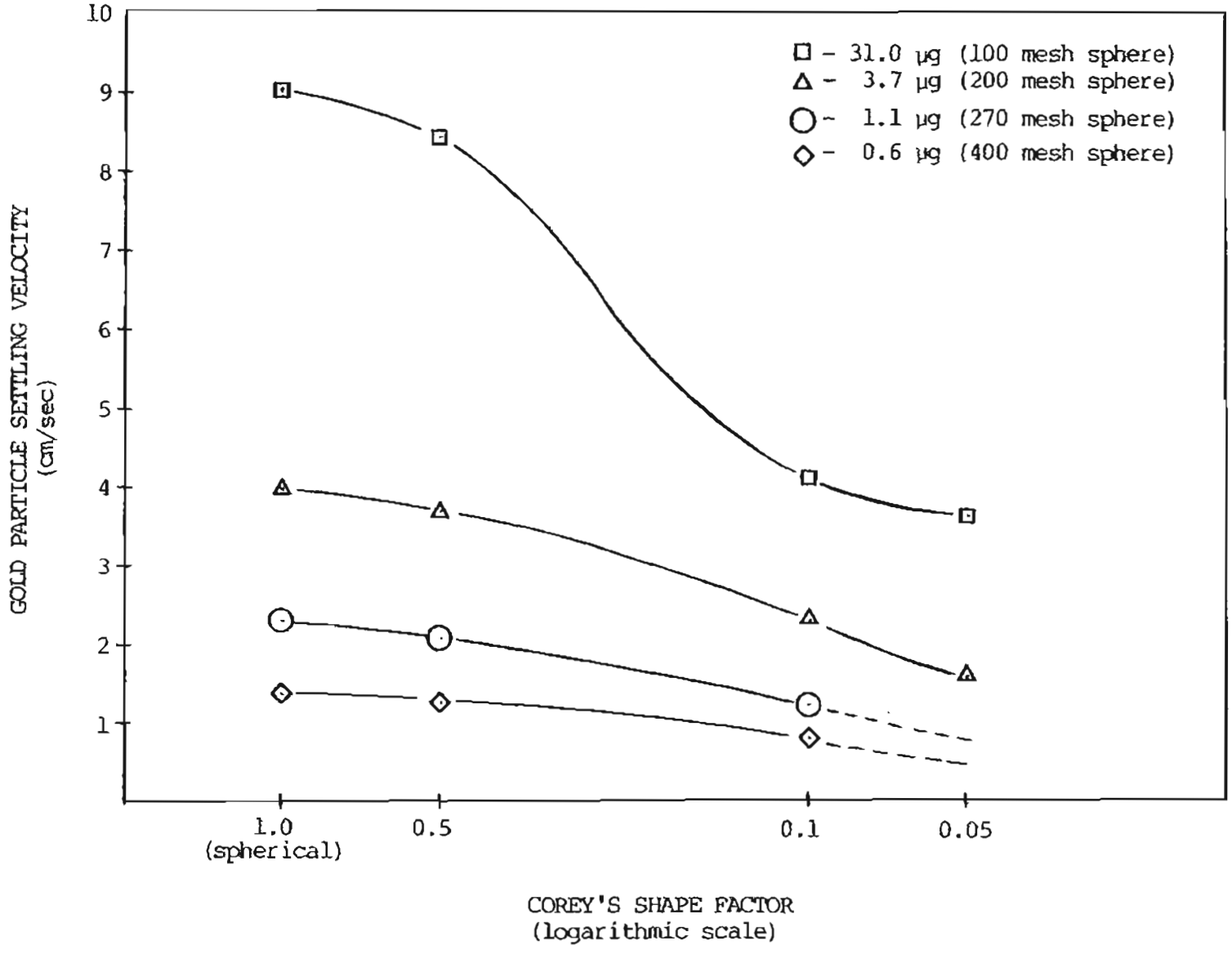


**Figure 14. Settling velocities for gold particles of constant mass at various flatnesses (31 µg to 0.6 µg).**

Table 6
Settling Velocities for Natural Placer Gold Particles
of Various Sizes and Shapes

| Particle Description (Nominal Size (ASTM Mesh) X Nominal Shape (CSF)) | Number of Natural Particles Observed (n) | Average Natural Particle Mass | 95% Confidence Interval* of mean Settling Velocity |
|---|---|---|---|
| 14 x 0.7 | 30 | 15.1 mg | 46.8 ± 2.7 |
| 14 x 0.1 | 30 | 3.1 mg | 18.4 ± 0.9 |
| 50 x 0.7 | 30 | 231 µg | 17.9 ± 0.6 |
| 50 x 0.3 | 30 | 78 µg | 8.9 ± 0.4 |

* $\alpha = 0.05$ $t(\alpha/2, 29) = 2.045$

Table 7
Comparison of Mean Settling Velocities for Natural and
Manufactured Gold Particles of Similar Nominal Size and Shape

| Particle Description (Size x Shape) | Particle Mass N | Particle Mass M | Mass Ratio (N/M) | Mean Settling Velocity (cm/sec) N | Mean Settling Velocity (cm/sec) M | Settling Velocity Ratio (N/M) |
|---|---|---|---|---|---|---|
| 14 x 0.7 | 15.1 mg | 21.0 mg | 71.6% | 46.8 | 68.8 | 68% |
| 14 x 0.1 | 3.1 mg | 2.5 mg | 123.1% | 18.4 | 17.3 | 106% |
| 50 x 0.7 | 231 µg | 241 µg | 95.8% | 17.9 | 19.7 | 91% |
| 50 x 0.3 | 78 µg | 110 µg | 70.9% | 8.9 | 10.8 | 82% |

N = natural
M = manufactured

Table 8
4 way ANOVA of Phase 4 data

| Source of Variation | df | MS | Ftest | F* | Comment |
|---|---|---|---|---|---|
| Main Effects | 12 | 7483.8 | 24050.2 | | |
| A. Temperature | 1 | 109.7 | 352.4 | 9.8 | $p < 0.001$ |
| B. Clay Mineralogy | 1 | 1603.5 | 5153.1 | 9.8 | $p < 0.001$ |
| C. Clay Concentration | 3 | 752.0 | 2416.8 | 5.1 | $p < 0.001$ |
| D. Blocks (8 gold size-shape combinations) | 7 | 12262.3 | 39406.6 | 3.4 | $p < 0.001$ |
| 2 Way Interactions | 42 | 56.2 | 180.5 | | |
| A X B | 1 | 2.9 | 9.3 | 9.8 | n.s. |
| A X C | 3 | 4.3 | 13.9 | 5.1 | $p < 0.001$ |
| A X D | 7 | 6.4 | 20.7 | 3.4 | $p < 0.001$ |
| B X C | 3 | 544.8 | 1750.9 | 5.1 | $p < 0.001$ |
| B X D | 7 | 26.6 | 85.5 | 3.4 | $p < 0.001$ |
| C X D | 21 | 22.7 | 73.1 | 2.3 | $p < 0.001$ |
| 3 Way Interactions | 52 | 7.8 | 25.0 | | |
| A X B X C | 3 | 0.7 | 2.4 | 5.1 | n.s. |
| A X B X D | 7 | 1.7 | 5.4 | 3.4 | $p < 0.001$ |
| A X C X D | 21 | 0.9 | 2.9 | 2.3 | $p < 0.001$ |
| B X C X D | 21 | 17.7 | 57.0 | 2.3 | $p < 0.001$ |
| 4 Way Interactions | 21 | 0.6 | 2.0 | | |
| A X B X C X D | 21 | 0.6 | 2.0 | 2.3 | n.s. |
| Treatments | 127 | 729.0 | 2342.7 | 1.7 | $p < 0.001$ |
| Residual | 128 | 0.3 | | | |
| Total | 255 | 363.2 | | | |

Bonferroni B = 15, $\alpha = 0.05$, $(1 - \alpha/B) = 0.997$
$F(1, 128, 0.997) \leq 9.8$
$F(3, 128, 0.997) \leq 5.1$
$F(7, 128, 0.997) \leq 3.4$
$F(21, 128, 0.997) \leq 2.3$
$F(127, 128, 0.997) \leq 1.7$

significant heteroscedacity was indicated. As noted earlier, this was expected due to the large variance differences between blocks. Because of the significant three way interactions, the data was broken down by blocks and plotted in Figures 15 through 22. Note that the manufactured gold particles used in the tests are referred to as "synthetic gold" in Figures 15-18.

Settling velocity data for phase 4 is presented in Tables A1-A8 of the appendix. Because of the heteroscedacity present ($p<0.001$), separate ANOVA's were run for each block (gold size-shape combination). Tables A1-A8 include the squared, pooled standard errors ($S^2$) from these ANOVA's as well as the Tukey T value at a 95% level of confidence ($\alpha = 0.05$) for within block pairwise comparisons. Bartlett Box F tests, to check for within block heteroscedacity, were also run.

Data, on the physical properties of the suspension samples taken throughout the generalized block testing, are shown in Tables 9 and 10. Because of the variations in temperature and also due to the variations in suspended solids concentrations between the cold and ambient factor levels within a block, it is difficult to interpret the statistically significant temperature effect observed from the analysis. It may be a shadow of the concentration differences. However,

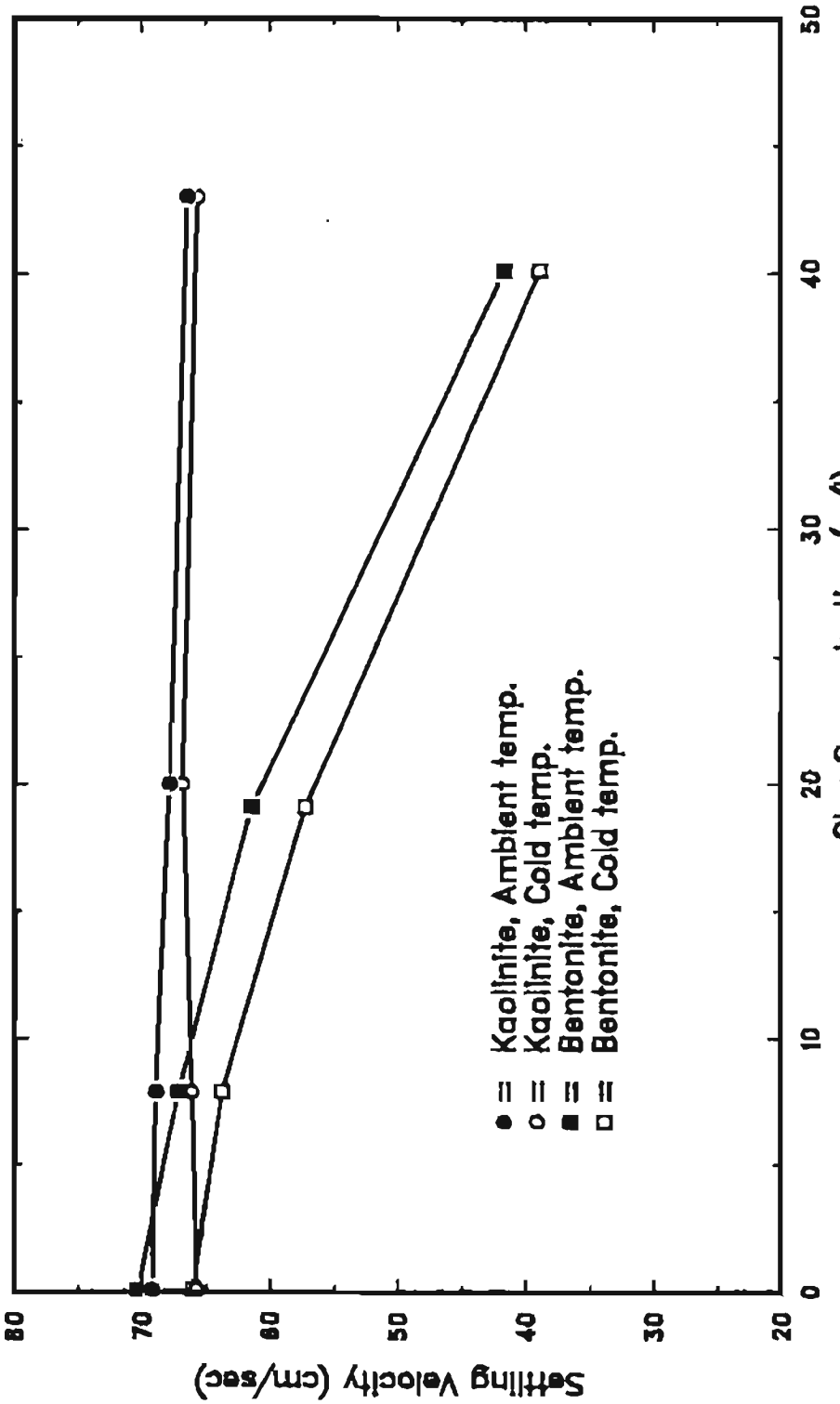


Figure 15. Factorial Data for Synthetic 14 x 0.7 Gold

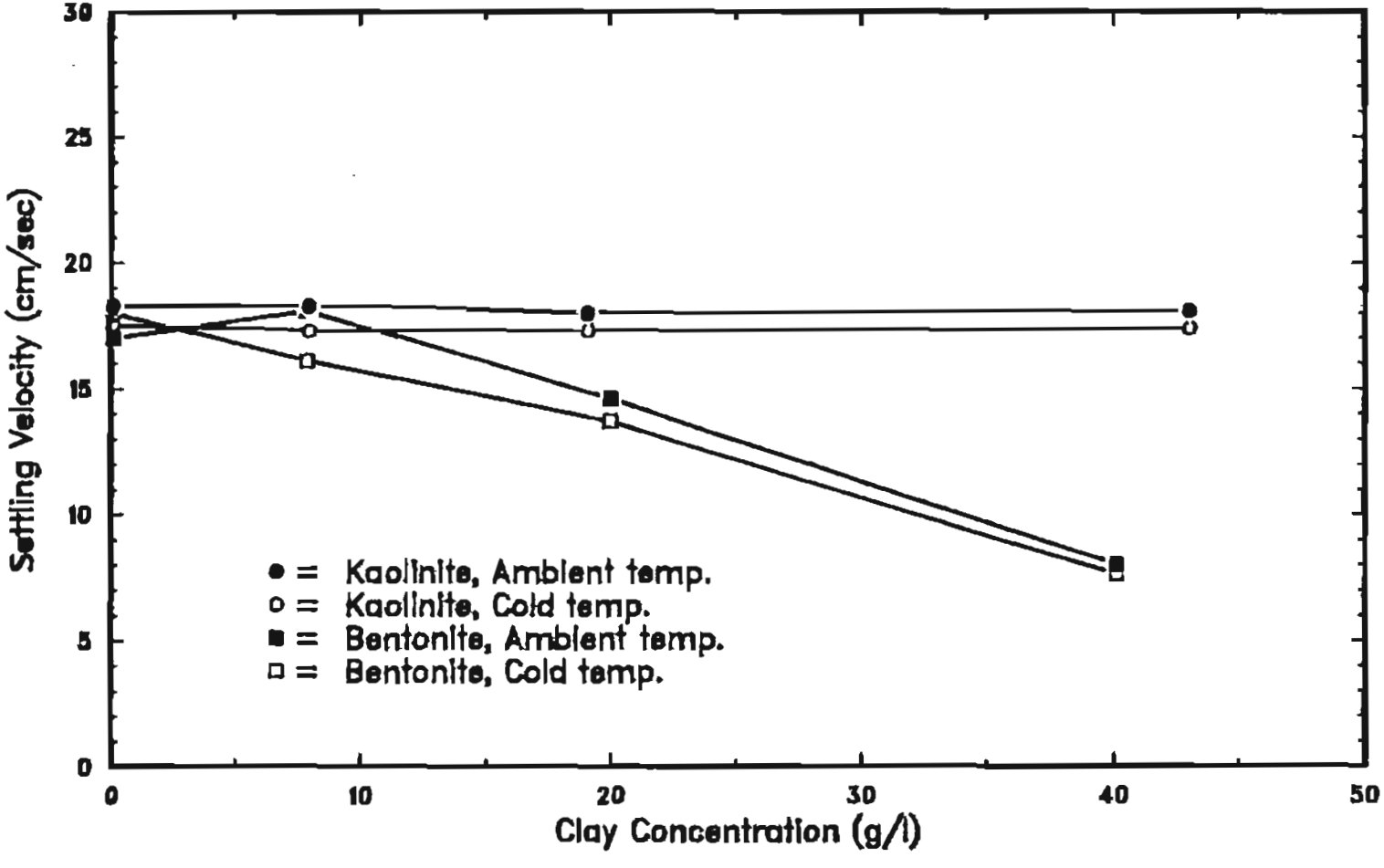


Figure 16. Factorial Data for Synthetic 14 x 0.1 Gold

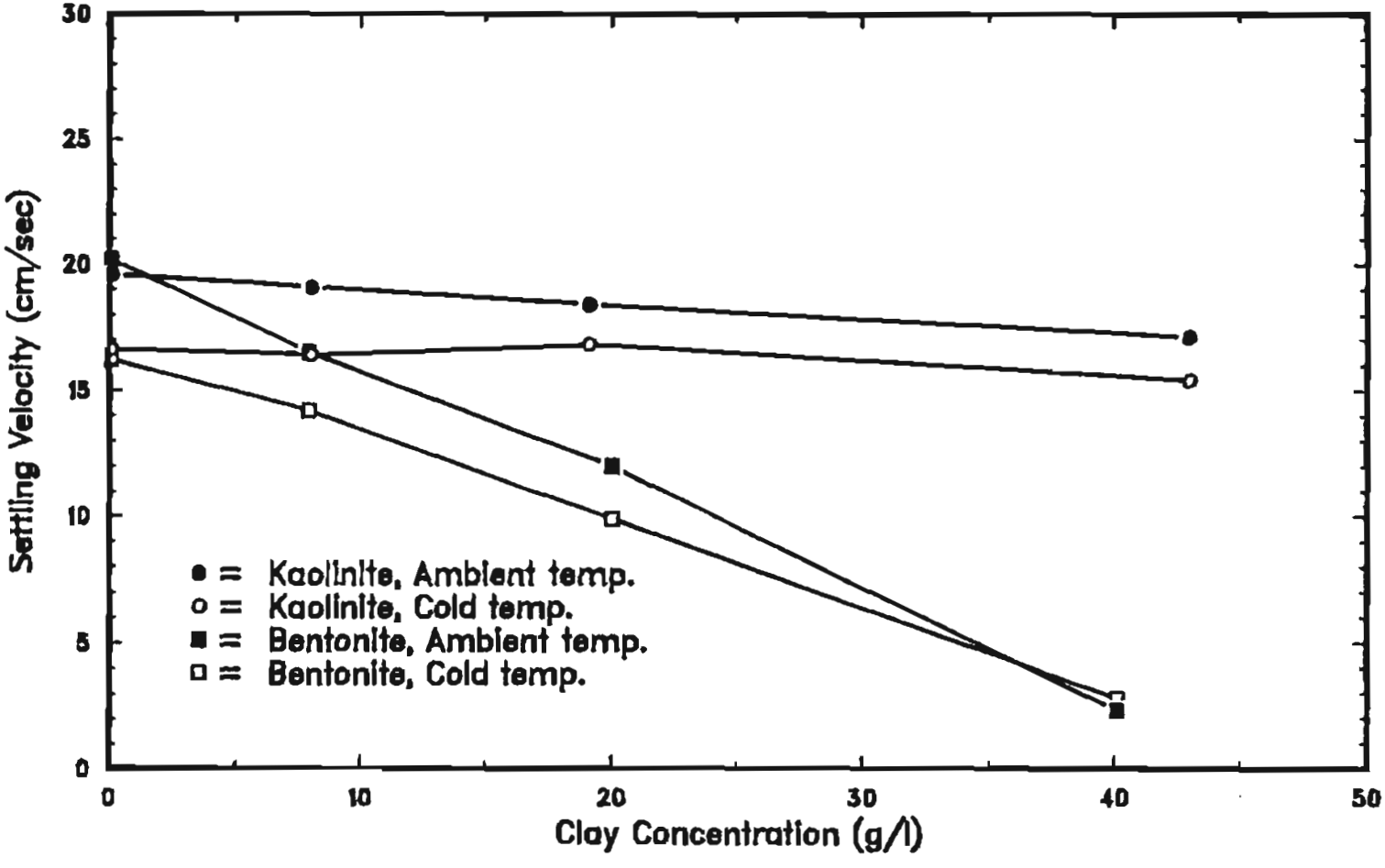


Figure 17. Factorial Data for Synthetic 50 x 0.7 Gold

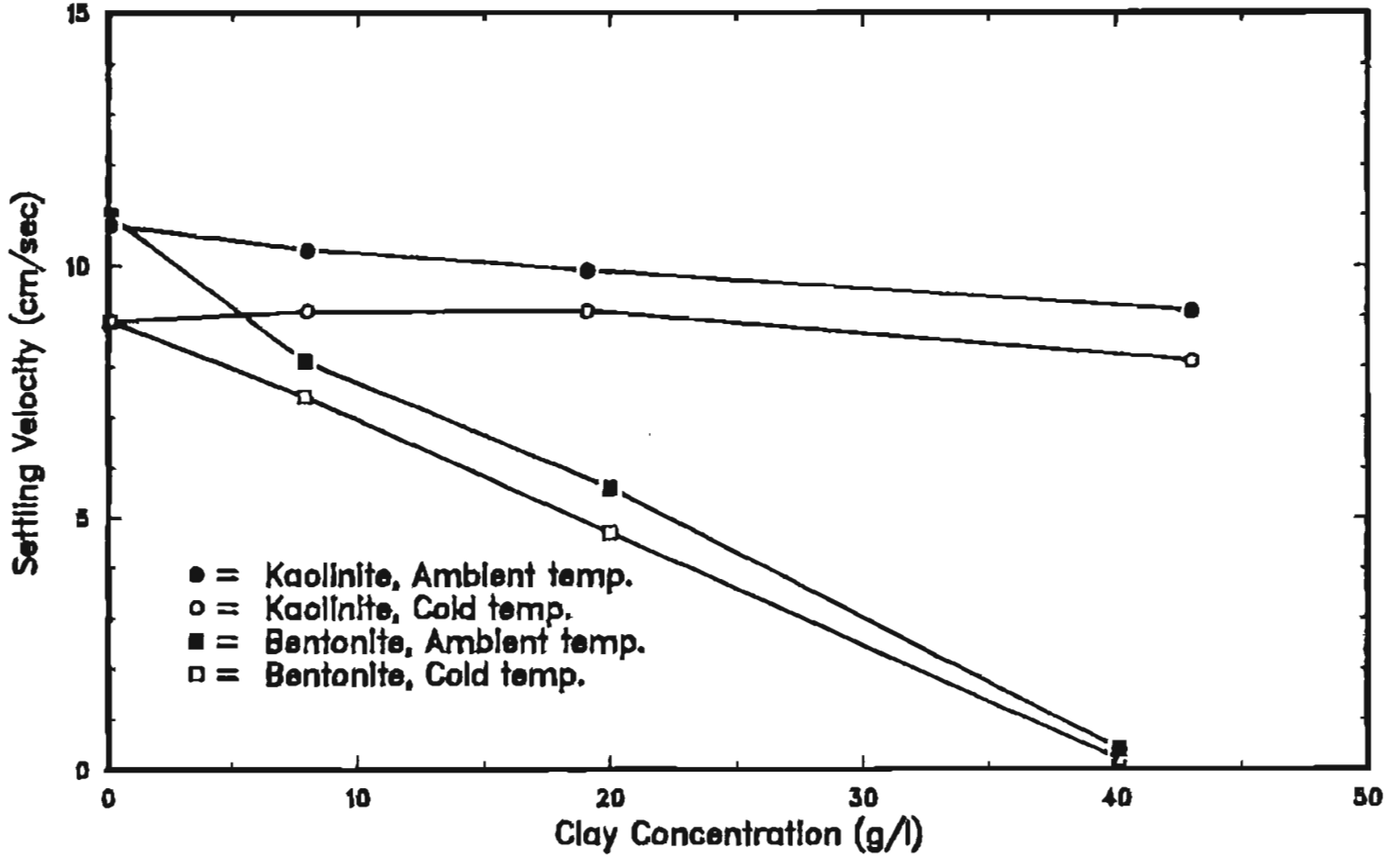


Figure 18. Factorial Data for Synthetic 50 x 0.3 Gold

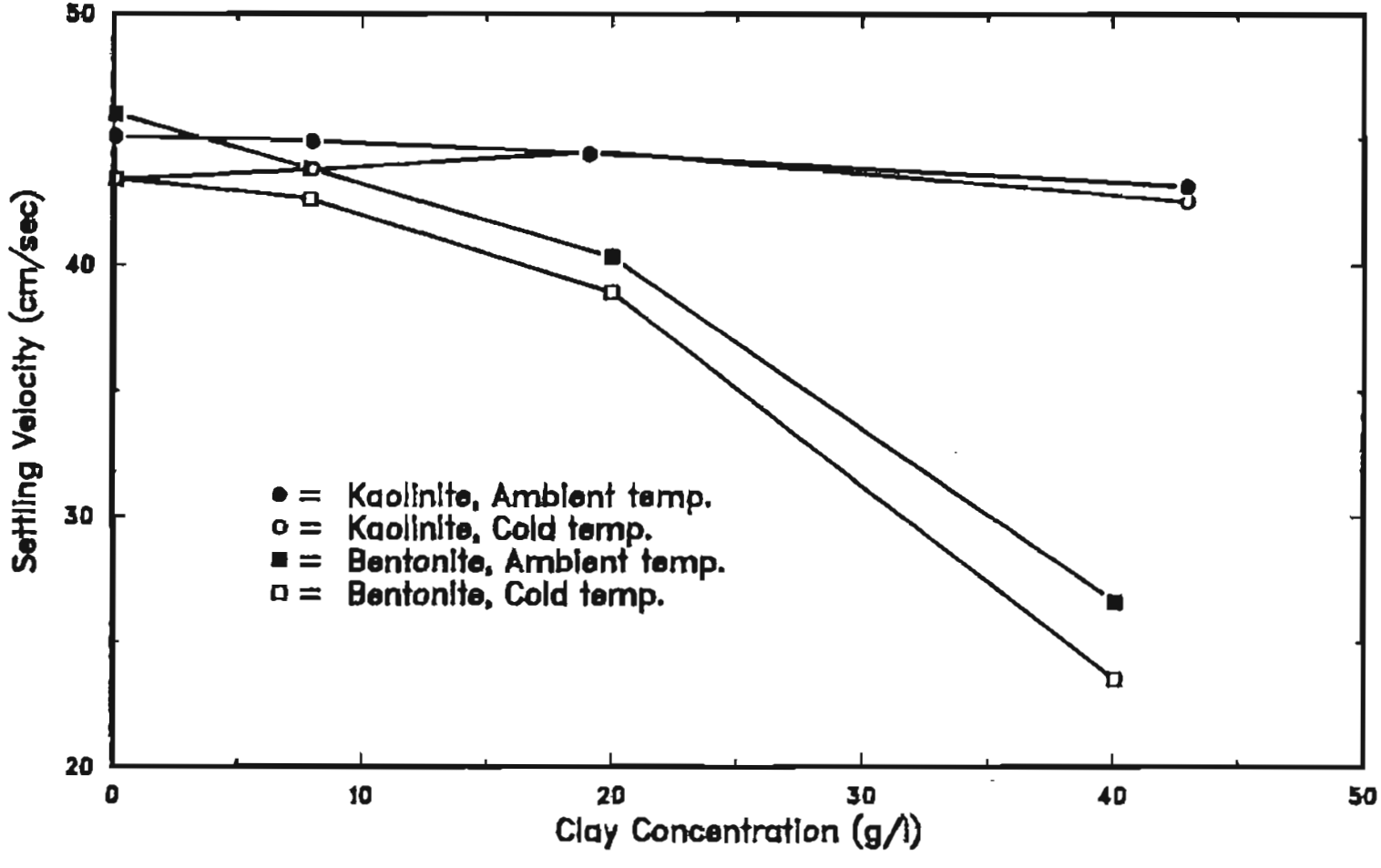


Figure 19. Factorial Data for Natural 14 x 0.7 Gold

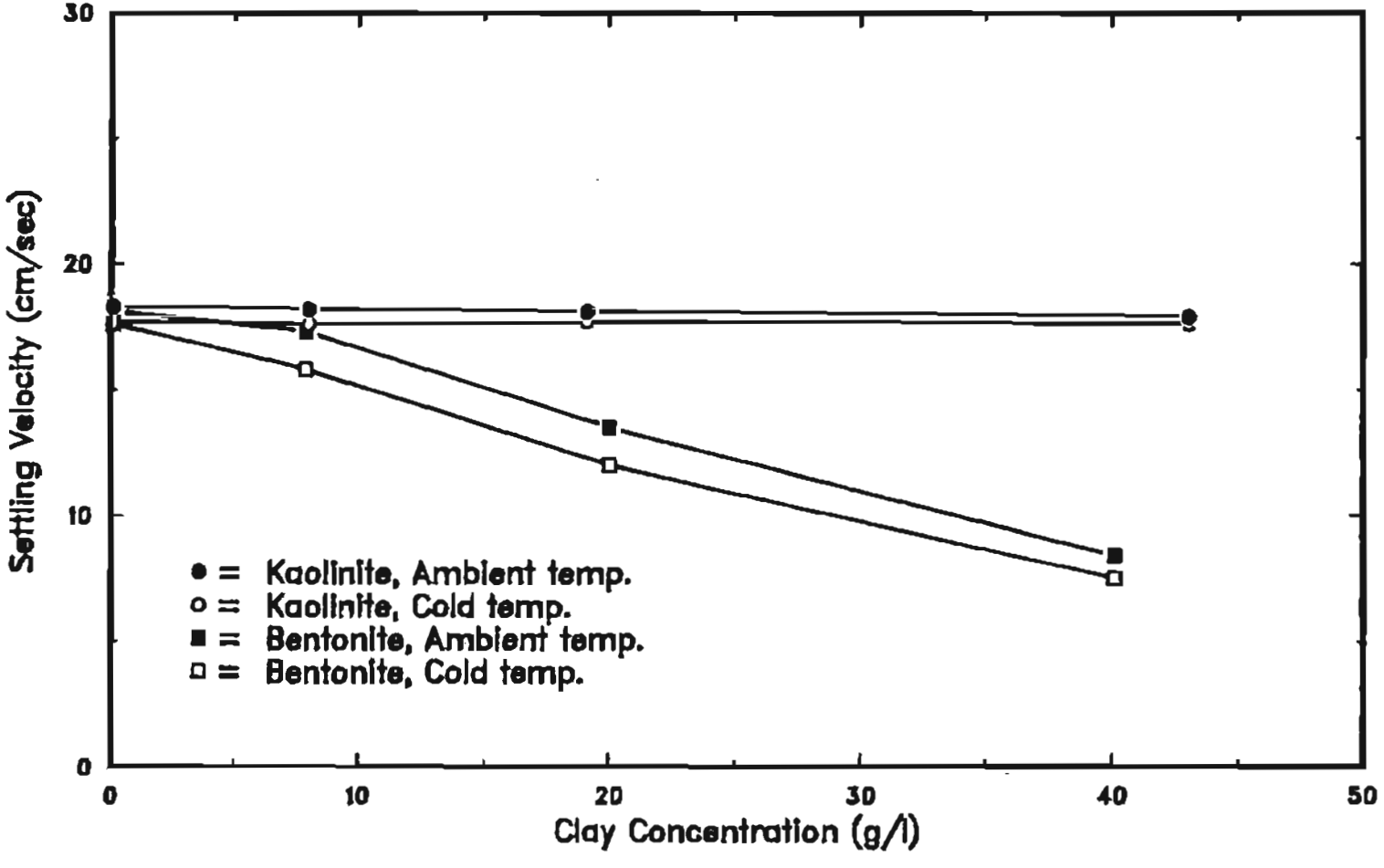


Figure 20. Factorial Data for Natural 14 x 0.1 Gold

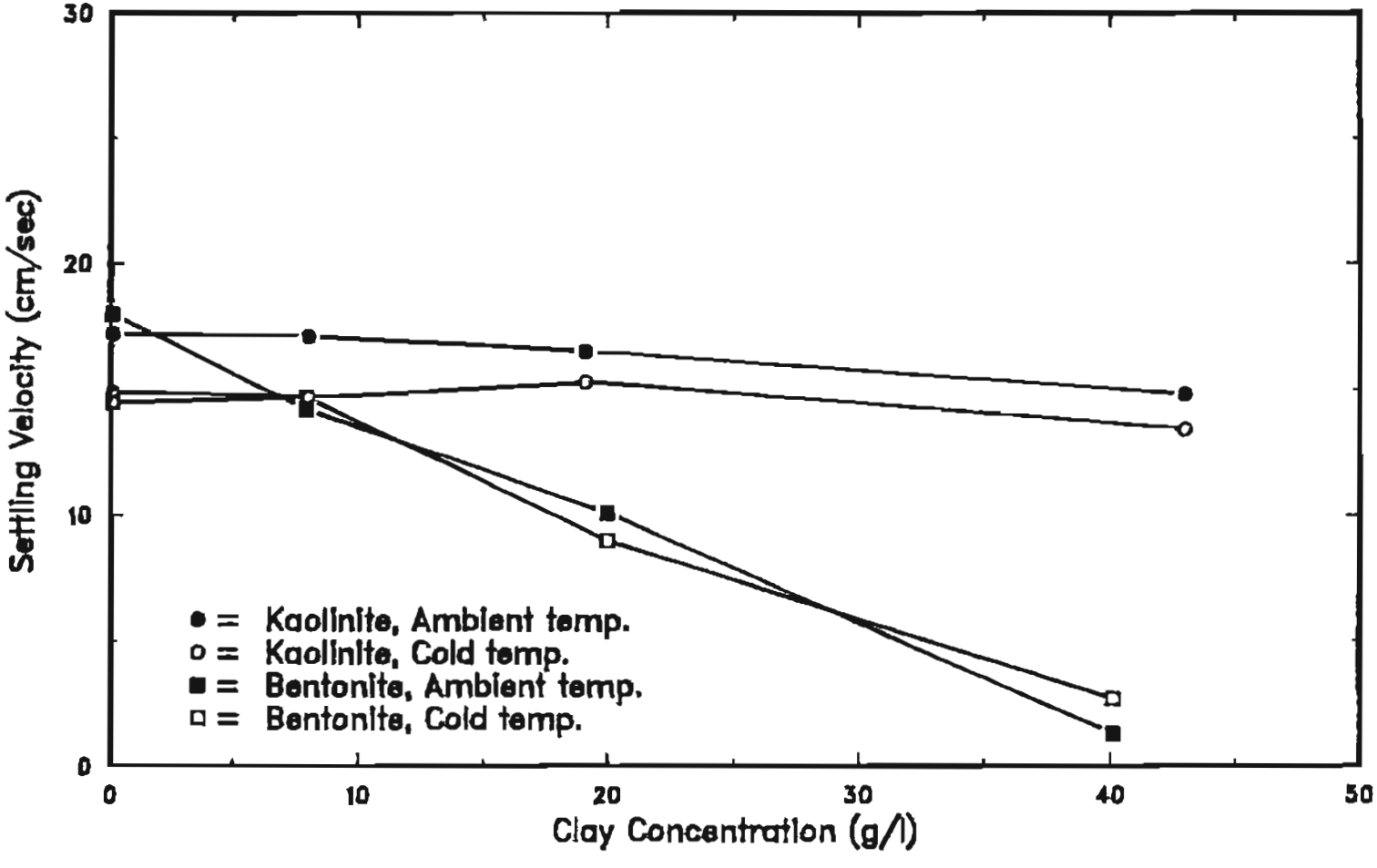


Figure 21. Factorial Data for Natural 50 x 0.7 Gold

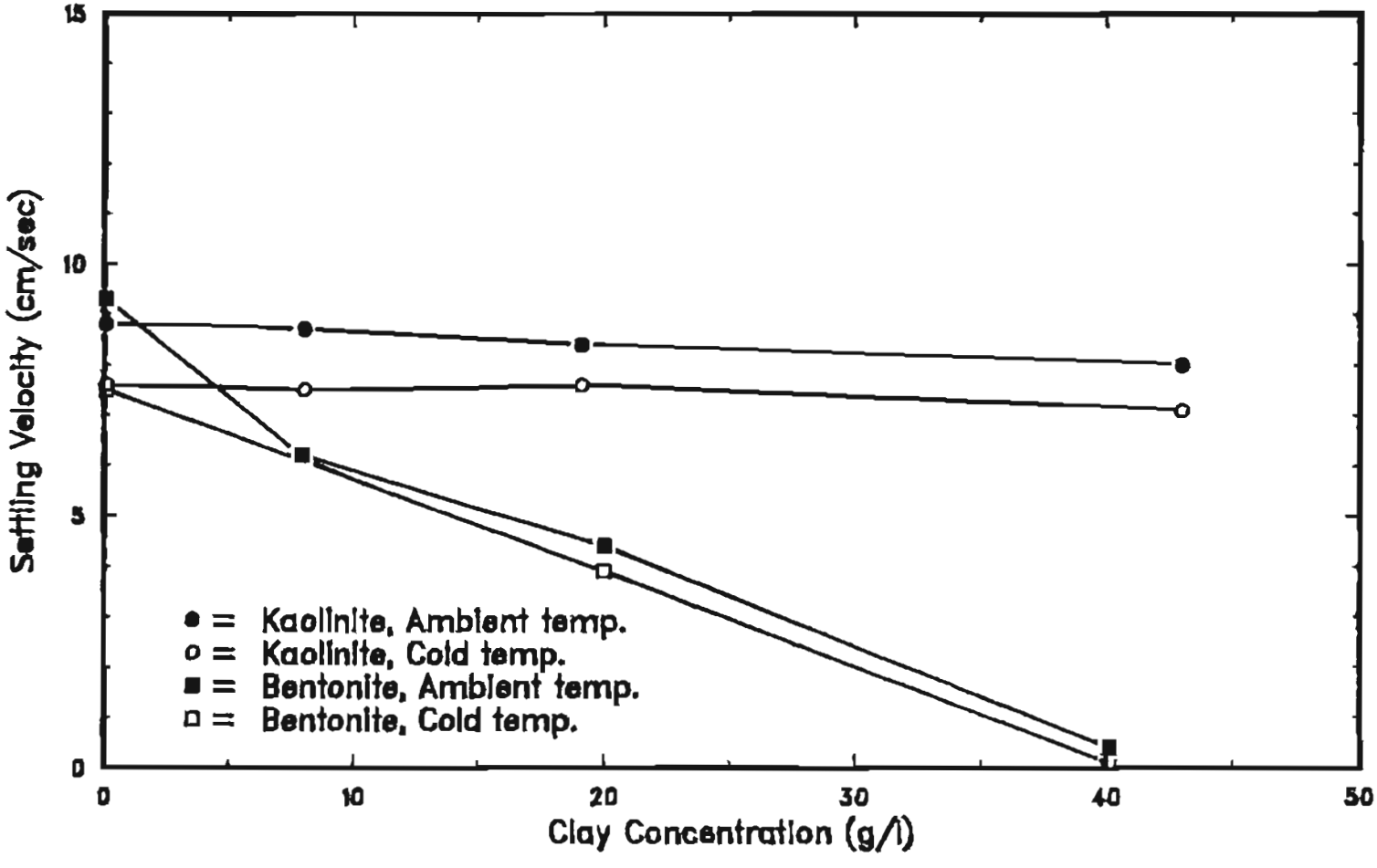


Figure 22. Factorial Data for Natural 50 x 0.3 Gold

Table 9
Physical Properties of Bentonite-Water Suspensions
Sampled During Phase 4 Testing

| Sample Number | Temp. (°C) | Suspended Solids Concentration (mg/l) per Sample | Suspended Solids Concentration (mg/l) 6 sample average | Turbidity (NTU) | Specific Gravity (at 6-sample average SS concentration) |
|---|---|---|---|---|---|
| 1A1 | 23 | 8,200 | | 1250 | |
| 1A2 | 22 | 7,200 | | 1300 | |
| 1A3 | 22 | 8,000 | 7900 | 1250 | 1.005 |
| 9C1 | 3 | 8,400 | | 1380 | |
| 9C2 | 5 | 8,200 | | 1360 | |
| 9C3 | 6 | 7,600 | | 1325 | |
| 2A1 | 22 | 21,000 | | 3000 | |
| 2A2 | 22 | 20,200 | | 2900 | |
| 2A3 | 22 | 20,000 | 20,000 | 2825 | 1.013 |
| 10C1 | 3 | 20,200 | | 3075 | |
| 10C2 | 6 | 19,500 | | 2950 | |
| 10C3 | 6 | 19,100 | | 2550 | |
| 3A1 | 19 | 42,000 | | 5625 | |
| 3A2 | 22 | 41,400 | | 5500 | |
| 3A3 | 23 | 41,500 | 40,100 | 6000 | 1.026 |
| 12C1 | 4 | 39,700 | | 5175 | |
| 12C2 | 4 | 38,600 | | 5125 | |
| 12C3 | 5 | 37,500 | | 5250 | |

the consistent settling velocity decrease observed between ambient and cold factor levels with only water as the fluid, suggests that the observed temperature influence may be in part real.

After the completion of all four phases of the study, six clay- water suspensions were made up; one for each of the 6-sample average levels seen in Tables 9 and 10. The viscosities of these suspensions were then determined at two temperature levels. As previously noted, a Fann Viscometer was used for these measurements. The apparent viscosity values obtained at various Fann shear rates are shown in Tables 11 and 12.

## CONCLUSIONS

Phases 1 through 3 have demonstrated the usefulness and accuracy of using a radiotracer detection system to determine settling velocities of gold particles. The graphs and tables produced by these three sections of this study should find application in gold recovery plant design.

The results of phase 4 have shown that not only the clay concentration in process water but more importantly its clay mineralogy will influence the settling velocity of fine gold significantly. The impact of mineralogy appears to be related to the variable viscosifying properties of clay minerals. It was shown earlier that the influence of increases in suspension density on gold's settling velocity is slight. Increases in suspension viscosity are theoretically very influential for gold particles settling at velocities below the Newtonian range. The results of phase 4 seem in part to substantiate the theory.

The data produced by this study may be further analyzed. This would expand the scope of this work. Some suggestions in this regard are presented in the following section.

## RECOMMENDATIONS

Due to the constraints of both time and funding the authors wish to recommend additional work which should

Table 10
Physical Properties of Kaolin-Water Suspensions
Sampled During Phase 4 Testing

| Sample Number | Temp. (°C) | Suspended Solids Concentration (mg/l) per Sample | Suspended Solids Concentration (mg/l) 6 sample average | Turbidity (NTU) | Specific Gravity (at 6-sample average SS concentration) |
|---|---|---|---|---|---|
| 16D1 | 19 | 8,800 | | 6,125 | |
| 16D2 | 20 | 8,300 | | 5,750 | |
| 16D3 | 20 | 7,800 | 8,000 | 5,875 | 1.005 |
| 7B1 | 4 | 8,500 | | 6,000 | |
| 7B2 | 7 | 7,500 | | 5,875 | |
| 7B3 | 8 | 7,100 | | 5,500 | |
| 13D1 | 18 | 20,400 | | 16,250 | |
| 13D2 | 19 | 19,500 | | 16,125 | |
| 13D3 | 19 | 19,600 | 19,100 | 16,500 | 1.012 |
| 6B1 | 8 | 19,900 | | 15,250 | |
| 6B2 | 10 | 18,300 | | 15,375 | |
| 6B3 | 11 | 17,000 | | 13,875 | |
| 15D1 | 15 | 49,100 | | 39,625 | |
| 15D2 | 18 | 39,000 | | 36,250 | |
| 15D3 | 19 | 42,000 | 43,000 | 37,000 | 1.028 |
| 8B1 | 3 | 44,800 | | 37,625 | |
| 8B2 | 10 | 42,800 | | 35,250 | |
| 8B3 | 10 | 40,200 | | 36,875 | |

be pursued with respect to this study. Some of these recommendations require only additional analysis of the data already generated by this project. These include but are not limited to:

1) Use the settling velocities obtained for gold particles to calculate their respective drag coefficients. Plot these against those given by Albertson[12] and compare.

2) Make multiple comparisons between the within block treatment levels of the phase 4 data in order to establish the statistical significance of between treatment settling velocity differences.

3) Calculate theoretical spherical settling velocities and compare them to the settling velocities for spherical gold particles generated in phase 1.

4) Plot rheograms for the clay-water suspensions sampled in phase 4.

The authors also wish to suggest additional laboratory and field work which should expand the scope of this study. This would include:

1) The use of a constant temperature bath with subsequent settling velocity tests to better control the system temperature.

2) Test additional clay mineralogies to determine their influence on the settling velocity of gold particles as their concentration in the fluid is increased.

3) Test additional manufactured and natural gold grains with respect to the new and previously tested clay mineralogies and concentrations. These should include both coarser and finer grains than those used by the authors in their present work.

4) Collect field samples of recycled placer mine

Table 11
Apparent Viscosities for Bentonite-Water Suspensions
at Various Fann Shear Rates.

| Apparent Suspended Solids Concentration (mg/l) | Fann Shear Temperature (°C) ambient/cold | Viscosity Fann Shear Rate (RPM) | Stress ($lb/100ft^2$) ambient/cold | ($\mu_a$ in centipoise) ambient/cold |
|---|---|---|---|---|
| | | 600 | 7.25/10.00 | 3.6/5.0 |
| | | 300 | 4.00/5.50 | 4.0/5.5 |
| | | 200 | 3.25/4.00 | 4.9/6.0 |
| 40,100 | 19/5 | 100 | 2.00/2.25 | 6.0/6.8 |
| | | 6 | 0.25/0.25 | 12.5/12.5 |
| | | 3 | 0.25/0.25 | 25.0/25.0 |
| | | 600 | 4.00/6.00 | 2.0/3.0 |
| | | 300 | 2.25/3.25 | 2.2/3.2 |
| 20,000 | 19/4.5 | 200 | 1.50/2.25 | 2.2/3.4 |
| | | 100 | 1.00/1.25 | 3.0/3.8 |
| | | 6 | 0.25/0.25 | 12.5/12.5 |
| | | 3 | 0.00/0.00 | — |
| | | 600 | 3.00/4.25 | 1.5/2.1 |
| | | 300 | 1.75/2.25 | 1.8/2.2 |
| 7,900 | 18/4.5 | 200 | 1.25/1.50 | 1.9/2.2 |
| | | 100 | 0.75/0.90 | 2.2/2.7 |
| | | 6 | 0.00/0.00 | — |
| | | 3 | 0.00/0.00 | — |
| | | 600 | 2.00/3.00 | 1.0/1.5 |
| Tap-Water | 23/7 | 300 | 1.00/1.50 | 1.0/1.5 |
| | | 200 | 0.75/1.00 | 1.1/1.5 |
| | | 100 | 0.25/0.50 | 0.8/1.5 |
| | | 6 | 0.00/0.00 | — |
| | | 3 | 0.00/0.00 | — |

Table 12
Apparent Viscosities for Kaolin-Water Suspensions
at Various Fann Shear Rates.

| Apparent Suspended Solids Concentration (mg/l) | Fann Shear Temperature (°C) ambient/cold | Viscosity Fann Shear Rate (RPM) | Stress ($lb/100ft^2$) ambient/cold | ($\mu_a$ in centipoise) ambient/cold |
|---|---|---|---|---|
| | | 600 | 2.75/3.75 | 1.4/1.9 |
| | | 300 | 1.50/2.00 | 1.5/2.0 |
| 43,000 | 18/5.5 | 200 | 1.00/1.25 | 1.5/1.9 |
| | | 100 | 0.75/0.75 | 2.2/2.2 |
| | | 6 | 0.00/0.00 | — |
| | | 3 | 0.00/0.00 | — |
| | | 600 | 2.25/3.50 | 1.1/1.8 |
| | | 300 | 1.25/1.75 | 1.2/1.8 |
| 19,100 | 18/5 | 200 | 1.00/1.25 | 1.5/1.9 |
| | | 100 | 0.50/0.75 | 1.5/2.2 |
| | | 6 | 0.00/0.00 | — |
| | | 3 | 0.00/0.00 | — |
| | | 600 | 2.25/3.25 | 1.1/1.6 |
| | | 300 | 1.20/1.75 | 1.2/1.8 |
| 8,000 | 18/5 | 200 | 0.90/1.00 | 1.4/1.5 |
| | | 100 | 0.50/0.50 | 1.5/1.5 |
| | | 6 | 0.00/0.00 | — |
| | | 3 | 0.00/0.00 | — |
| | | 600 | 2.00/3.00 | 1.0/1.5 |
| Tap-Water | 23/7 | 300 | 1.00/1.50 | 1.0/1.5 |
| | | 200 | 0.75/1.00 | 1.1/1.5 |
| | | 100 | 0.25/0.50 | 0.1/1.5 |
| | | 6 | 0.00/0.00 | — |
| | | 3 | 0.00/0.00 | — |

process water in order to determine its physical properties, i.e. suspended solids concentration, density and viscosity, as well as the size distribution of the suspended solids. Such field work should include tests to assess the plant's gold recovery as a function of suspension rheology.

## REFERENCES


1) Peterson, L.A., Tsigonis, R.C., Cronin, J.E., and Hanneman, K.L., "Investigation of the Effect of Total Suspended Solids Levels on Gold Recovery in a Pilot Scale Sluice", Report for Alaska State Department of Environmental Conservation, Sept. 1984, 43 p.

2) Walsh, D.E., "Evaluation of the Four Inch Compound Water Cyclone as a Fine Gold Concentrator Using Radiotracer Techniques", MIRL Report No. 70, University of Alaska, Fairbanks, 1985, 268 p.

3) Lashley, W.C., "Study No. 1, The Flatness Factor", American Society for Applied Technology, Silver City, New Mexico, 1983.

4) Shilo, N.A. and Shumilov, Yu. V., "New Experimental Data on Settling of Gold Particles in Water", Doklady Akademii Navk SSSR, 1970, vol. 195, no. 1, pp. 193-196.

5) Shumilov, Yu. V. and Shumovskiy, "Experimental Data on the Hydraulic Size of Some Placer Minerals in the Northeast USSR", Doklady Akademii Navk SSSR, 1975, vol. 225, no. 5, pp. 1174-1176.

6) Saks, S., Ye, "Principle of Hydrodynamic Equivalence of Clastic Particles", Vyssh, Ucheb. Zavedeniy IZVI, Geologiya i Razvedka, 1974, no. 11, pp. 84-88.

7) Tourtelot, H.A., "Hydraulic Equivalence of Grains of Quartz and Heavier Minerals, and Implications for the Study of Placers", Geologic Survey Professional paper 594-F, U.S. Government Printing Office, Washington, D.C., 1968.

8) Cook, D.J. and Rao, P.D., "Distribution, Analysis, and Recovery of Fine Placer Gold from Alluvial Deposits", Mineral Industry Research Laboratory, University of Alaska, Fairbanks, 1973.

9) Wasp, E.J., Kenny, J.P., and Gandhi, R.L., Solid-Liquid Flow Slurry Pipeline Transportation, Trans Tech Publications, Clausthal, Germany, 1977, pp. 33-59.

10) Heywood, H., "Calculation of the Specific Surface of a Powder", Institute of Mechanical Engineering Proceedings, 1933, vol. 125, pp. 383-459.

11) Corey, A.T., "Influence of Shape on the Fall Velocity of Sand Grains", Colorado A and M College (now Colorado State University), Fort Collins, Masters Thesis, 1949, 102 p.

12) Albertson, M.L., Schulz, E.F. and Welde, R.H., "Influence of Shape on the Fall Velocity of Sedimentary Particles", U.S. Army Corps of Engineers, Omaha, Nebraska, 1954, 163 p.

13) Kline, S.J. and McClintock, F.A., "Describing Uncertainties in Single Sample Experiments", Mechanical Engineering, Jan. 1953, p. 3.

14) Imco Services, Applied Mud Technology, The Haliburton Company, 1981.

15) McGuire, W.J., Holditch, S.A. and Rollins, J.T., Laboratory Manual for Petroleum Engineering 307, Texas A&M University, College Station, 1985, 85 p.

# APPENDIX

TABLE A1. FACTORIAL DATA FOR SYNTHETIC 14 X 0.7 GOLD.

| CLAY TYPE | WATER TEMPERATURE | CLAY CONCENTRATION | GOLD SETTLING VELOCITY (cm/sec) |
|---|---|---|---|
| KAOLINITE | AMBIENT | ZERO | 69.2 |
| | | LOW | 68.9 |
| | | MEDIUM | 67.8 |
| | | HIGH | 66.4 |
| | COLD | ZERO | 65.7 |
| | | LOW | 66.1 |
| | | MEDIUM | 66.8 |
| | | HIGH | 65.6 |
| BENTONITE | AMBIENT | ZERO | 70.3 |
| | | LOW | 67.1 |
| | | MEDIUM | 61.4 |
| | | HIGH | 41.7 |
| | COLD | ZERO | 66.0 |
| | | LOW | 63.7 |
| | | MEDIUM | 57.2 |
| | | HIGH | 38.9 |

Bartlett Box F Test: $p = 0.023$ $n = 2$

$S^2 = 0.77$

$T_{95} = 4.00$

$S(T_{95}) = 3.50$

TABLE A2. FACTORIAL DATA FOR SYNTHETIC 14 X 0.1 GOLD.

| CLAY TYPE | WATER TEMPERATURE | CLAY CONCENTRATION | GOLD SETTLING VELOCITY (cm/sec) |
|---|---|---|---|
| KAOLINITE | AMBIENT | ZERO | 18.3 |
| | | LOW | 18.3 |
| | | MEDIUM | 18.0 |
| | | HIGH | 18.1 |
| | COLD | ZERO | 17.5 |
| | | LOW | 17.3 |
| | | MEDIUM | 17.3 |
| | | HIGH | 17.4 |
| BENTONITE | AMBIENT | ZERO | 17.0 |
| | | LOW | 18.1 |
| | | MEDIUM | 14.6 |
| | | HIGH | 8.0 |
| | COLD | ZERO | 18.0 |
| | | LOW | 16.1 |
| | | MEDIUM | 13.7 |
| | | HIGH | 7.6 |

Bartlett Box F Test: $p = 0.069$ $n = 2$

$S^2 = 0.063$

$T_{95} = 4.00$

$S(T_{95}) = 1.00$

**TABLE A3. FACTORIAL DATA FOR SYNTHETIC 50 X 0.7 GOLD.**

| CLAY TYPE | WATER TEMPERATURE | CLAY CONCENTRATION | GOLD SETTLING VELOCITY (cm/sec) |
|---|---|---|---|
| KAOLINITE | AMBIENT | ZERO | 19.6 |
| | | LOW | 19.1 |
| | | MEDIUM | 18.4 |
| | | HIGH | 17.1 |
| | COLD | ZERO | 16.6 |
| | | LOW | 16.4 |
| | | MEDIUM | 16.8 |
| | | HIGH | 15.4 |
| BENTONITE | AMBIENT | ZERO | 20.2 |
| | | LOW | 16.5 |
| | | MEDIUM | 12.0 |
| | | HIGH | 2.3 |
| | COLD | ZERO | 16.2 |
| | | LOW | 14.2 |
| | | MEDIUM | 9.9 |
| | | HIGH | 2.8 |

Bartlett Box F Test: $p = 0.671$ $n = 2$

$S^2 = 0.048$

$T_{95} = 4.00$

$S(T_{95}) = 0.88$

TABLE A4. FACTORIAL DATA FOR SYNTHETIC 50 X 0.3 GOLD.

| CLAY TYPE | WATER TEMPERATURE | CLAY CONCENTRATION | GOLD SETTLING VELOCITY (cm/sec) |
|---|---|---|---|
| KAOLINITE | AMBIENT | ZERO | 10.8 |
| | | LOW | 10.3 |
| | | MEDIUM | 9.9 |
| | | HIGH | 9.1 |
| | COLD | ZERO | 8.9 |
| | | LOW | 9.1 |
| | | MEDIUM | 9;1 |
| | | HIGH | 8.1 |
| BENTONITE | AMBIENT | ZERO | 11.0 |
| | | LOW | 8.1 |
| | | MEDIUM | 5.6 |
| | | HIGH | 0.4 |
| | COLD | ZERO | 8.9 |
| | | LOW | 7.4 |
| | | MEDIUM | 4.7 |
| | | HIGH | 0.2 |

Bartlett Box F Test: $p = 0.378$ $n = 2$

$S^2 = 0.018$

$T_{95} = 4.00$

$S(T_{95}) = 0.537$

TABLE A5. FACTORIAL DATA FOR NATURAL
14 X 0.7 GOLD.

| CLAY TYPE | WATER TEMPERATURE | CLAY CONCENTRATION | GOLD SETTLING VELOCITY (cm/sec) |
|---|---|---|---|
| KAOLINITE | AMBIENT | ZERO | 45.1 |
| | | LOW | 44.9 |
| | | MEDIUM | 44.4 |
| | | HIGH | 43.1 |
| | COLD | ZERO | 43.4 |
| | | LOW | 43.8 |
| | | MEDIUM | 44.5 |
| | | HIGH | 42.5 |
| BENTONITE | AMBIENT | ZERO | 46.0 |
| | | LOW | 43.8 |
| | | MEDIUM | 40.3 |
| | | HIGH | 26.6 |
| | COLD | ZERO | 43.4 |
| | | LOW | 42.6 |
| | | MEDIUM | 38.9 |
| | | HIGH | 23.5 |

Bartlett Box F Test: $p = 0.132$ $n = 2$
$S^2 = 0.189$
$T_{95} = 4.00$
$S(T_{95}) = 1.74$

**TABLE A6. FACTORIAL DATA FOR NATURAL 14 X 0.1 GOLD.**

| CLAY TYPE | WATER TEMPERATURE | CLAY CONCENTRATION | GOLD SETTLING VELOCITY (cm/sec) |
|---|---|---|---|
| KAOLINITE | AMBIENT | ZERO | 18.3 |
| | | LOW | 18.2 |
| | | MEDIUM | 18.1 |
| | | HIGH | 17.9 |
| | COLD | ZERO | 17.7 |
| | | LOW | 17.6 |
| | | MEDIUM | 17.7 |
| | | HIGH | 17.6 |
| BENTONITE | AMBIENT | ZERO | 18.1 |
| | | LOW | 17.3 |
| | | MEDIUM | 13.5 |
| | | HIGH | 8.4 |
| | COLD | ZERO | 17.6 |
| | | LOW | 15.8 |
| | | MEDIUM | 12.0 |
| | | HIGH | 7.5 |

Bartlett Box F Test: $p = 0.004$ $n = 2$

$S^2 = 0.057$

$T_{95} = 4.00$

$S(T_{95}) = 0.96$

TABLE A7. FACTORIAL DATA FOR NATURAL 50 X 0.7 GOLD.

| CLAY TYPE | WATER TEMPERATURE | CLAY CONCENTRATION | GOLD SETTLING VELOCITY (cm/sec) |
|---|---|---|---|
| KAOLINITE | AMBIENT | ZERO | 17.2 |
| | | LOW | 17.1 |
| | | MEDIUM | 16.5 |
| | | HIGH | 14.8 |
| | COLD | ZERO | 14.9 |
| | | LOW | 14.7 |
| | | MEDIUM | 15.3 |
| | | HIGH | 13.4 |
| BENTONITE | AMBIENT | ZERO | 18.0 |
| | | LOW | 14.2 |
| | | MEDIUM | 10.1 |
| | | HIGH | 1.3 |
| | COLD | ZERO | 14.5 |
| | | LOW | 12.7 |
| | | MEDIUM | 9.0 |
| | | HIGH | 2.7 |

Bartlett Box F Test: $p = 0.297$ $n = 2$

$S^2 = 0.081$

$T_{95} = 4.00$

$S(T_{95}) = 1.14$

**TABLE A8. FACTORIAL DATA FOR NATURAL 50 X 0.3 GOLD.**

| CLAY TYPE | WATER TEMPERATURE | CLAY CONCENTRATION | GOLD SETTLING VELOCITY (cm/sec) |
|---|---|---|---|
| KAOLINITE | AMBIENT | ZERO | 8.8 |
| | | LOW | 8.7 |
| | | MEDIUM | 8.4 |
| | | HIGH | 8.0 |
| | COLD | ZERO | 7.6 |
| | | LOW | 7.5 |
| | | MEDIUM | 7.6 |
| | | HIGH | 7.1 |
| BENTONITE | AMBIENT | ZERO | 9.3 |
| | | LOW | 6.2 |
| | | MEDIUM | 4.4 |
| | | HIGH | 0.4 |
| | COLD | ZERO | 7.5 |
| | | LOW | 6.1 |
| | | MEDIUM | 3.9 |
| | | HIGH | 0.1 |

Bartlett Box F Test: $p = 0.519$ $n = 2$

$S^2 = 0.023$

$T_{95} = 4.00$

$S(T_{95}) = 0.61$